Patterns of (trace) metals and microorganisms in the Rainbow hydrothermal vent plume at the Mid-Atlantic Ridge

Sabine Haalboom[1,*], David M. Price[1,*,#], Furu Mienis[1], Judith D.L van Bleijswijk[1], Henko C. de Stigter[1], Harry J. Witte[1], Gert-Jan Reichart[1,2], Gerard C.A. Duineveld[1]

[1] NIOZ Royal Netherlands Institute for Sea Research, department of Ocean Systems, and Utrecht University, PO Box 59, 1790 AB Den Burg, Texel, The Netherlands

[2] Utrecht University, Faculty of Geosciences, 3584 CD Utrecht, The Netherlands

[*] These authors contributed equally to this work

[#] Current address: University of Southampton, Waterfront Campus, European Way, Southampton, UK, SO14 3ZH.

sabine.haalboom@nioz.nl; D.M.Price@soton.ac.uk

Keywords: Rainbow vent; Epsilonproteobacteria; Hydrothermal vent plume; Deep-sea mining; Rare earth elements; Seafloor massive sulfides

Abstract

Hydrothermal vent fields found at mid-ocean ridges emit hydrothermal fluids which disperse as neutrally buoyant plumes. From these fluids seafloor massive sulfides (SMS) deposits are formed which are being explored as possible new mining sites for (trace) metals and rare earth elements (REEs). It has been suggested that during mining activities large amounts of suspended matter will appear in the water column due to excavation processes, and due to discharge of mining waste from the surface vessel. Understanding how hydrothermal plumes can be characterised by means of geochemistry and microbiology as they spread away from their source and how they affect their surrounding environment may help in characterising the behaviour of the dilute distal part of chemically enriched mining plumes.

This study on the extensive Rainbow hydrothermal plume, observed up to 25 km downstream from the vent site, enabled us to investigate how microbial communities and (trace) metal composition change in a natural plume with distance. The (trace) metal and REE content of suspended particulate matter (SPM) was determined using sector field inductively coupled plasma mass spectrometry (SF-ICP-MS) with high resolution (HR) and the microbial communities of the neutrally buoyant plume, above plume-, below plume-, and near-bottom water and sediment were characterised by using 16S rRNA amplicon sequencing methods. Both vertically in the water column and horizontally along the neutrally buoyant plume, geochemical and biological changes were evident as the neutrally buoyant plume stood out by its enrichments in (trace) metals and REEs as e.g. Fe, Cu, V, Mn and REEs were enriched by factors of up to ~80, ~90, ~52, ~2.5 and ~40 respectively, compared to above plume water samples taken at 1000 m water depth. The concentrations of these elements changed as the plume aged shown by the decrease of element/Fe molar ratios of chalcophile elements (Cu, Co, Zn), indicative of rapid removal from the hydrothermal plume or removal from the solid phase. Conversely, increasing REE/Fe molar ratios imply uptake of REEs from the ambient seawater onto Fe-oxyhydroxides. This was also reflected in the background pelagic system as Epsilonproteobacteria started to dominate and univariate microbial biodiversity declined with distance away from the Rainbow hydrothermal vent field. The Rainbow hydrothermal plume provides a geochemically enriched natural environment, which is a heterogeneous, dynamic habitat that is conducive to ecological changes in a short time span. This study of a hydrothermal plume provides a baseline study to characterize the natural plume before the interference of deep-sea mining.

1 Introduction

Hydrothermal vent fields found at mid-ocean ridges and back-arc basins are known for discharging fluids rich in potential microbial energy sources such as H_2, H_2S, CH_4, NH_4 and Fe (Jannasch and Mottl, 1985; McCollom, 2000). In addition, they are characterised by the presence of polymetallic sulfide deposits containing high grades of metals like Cu, Co, Zn and rare earth elements (REEs) (Cave et al., 2002; Chavagnac et al., 2005). Because of the steadily increasing demand for these metals, and their geo-

political distribution on land, hydrothermal vent deposits are explored as new mining sites (Hoagland, 2010). Since such areas accommodate unique and vulnerable marine life, serious concerns exist about the environmental sustainability of seafloor massive sulfide (SMS) deposit mining (Boschen et al., 2013; Collins et al., 2013), especially with regards to the effects of the different plumes, which are generated during the excavation of ores and by the return flow of wastes in the vicinity of hydrothermal vents (Ramirez-Llodra et al., 2011; Vare et al., 2018). As SMS mining will concentrate on deposits around hydrothermal vents, and not on active vents or chimneys due to technical risks associated with high temperatures (Gwyther et al., 2008), it is likely that the background and extinct vent communities (from microorganisms to megafauna) will be impacted through habitat loss, mechanical destruction, noise, smothering and bioaccumulation of toxic substances (Levin et al., 2016). However, knowledge about the background ecosystem and natural plume is sparse, as the vents and their proximal fauna have attracted most of the attention, for example in microbiology (e.g. Han et al., 2018; Cerqueira et al., 2018).

To fill this gap, the Dutch TREASURE project (STW-NWO) was focussed on describing the structure of the background pelagic and benthic communities of an active hydrothermal vent site with SMS deposits on the Mid-Atlantic Ridge (MAR). The Rainbow hydrothermal vent (36°14" N on the MAR) was selected for this study as it ejects one of the most prominent and persistent natural plumes on the MAR. Hydrothermal plumes represent a distinct natural ecosystem in itself, which under the influence of currents may extend tens of kilometres away from its point of origin. Basic knowledge of natural plumes is essential to be able to discern impacts arising from future SMS mining plumes created in the vicinity of the hydrothermal vent which are likely interfere with the natural hydrothermal plume. Though mining plumes will have a higher initial density and therefore tend to sink rather than maintain buoyancy (Gwyther et al., 2008; Boschen et al., 2013), the finest and slowest sinking fraction of suspended solids in the mining plume may interfere with the natural plume during its dispersal, especially when released above the seafloor.

Since the discovery of the Rainbow hydrothermal vent field in 1996 by German et al., several studies concerning the composition of the hydrothermal fluid and the sediment influenced by fall-out of particulates from the Rainbow and other hydrothermal plumes have been published. These showed, for

example, that the underlying host rock influences the hydrothermal fluid composition (Wetzel and Shock, 2000; Marques et al., 2006). Geochemical investigation of sediment by Cave et al. (2002) at distances of 2 to 25 km from the Rainbow hydrothermal vent field showed enrichments of Fe, Cu, Mn, V, As and P, as well as REEs (Chavagnac et al., 2005) as a result of fallout from the hydrothermal plume. It has further been shown that microbial activity influences geochemical processes in the plume (Breier et al., 2012; Dick et al., 2013), such as scavenging and oxidation of metals (Cowen and Bruland, 1985; Cowen et al., 1990; Mandernack and Tebo, 1993; Dick et al., 2009), influencing the local ocean geochemistry.

Microbial activity within the plume is fuelled by redox reactions that provide energy for chemolithoautotrophic microbial taxa. The abundance of energy sources within plumes and hydrothermal systems support a plethora of chemolithoautotrophic microbial communities (e.g. Orcutt et al., 2011; Frank et al., 2013; Anantharaman et al., 2016). Plume microbial communities can be distinct or relatively similar to background communities (Dick and Tebo et al., 2010; Sheik et al., 2015; Olins et al., 2017), with plume associated bacteria originating from either seafloor communities, background seawater communities or from growth within the plume (Dick et al., 2013). Djurhuus et al. (2017) observed the reduction in dominance of vent associated microorganisms with increased redox potential, suggesting that communities associated with the initial rising plume become diluted on a scale of metres. Comparatively little is known about changes in chemical composition and microbial assemblages in the hydrothermal plume after its initial rise, when it becomes neutrally buoyant and is dispersed by currents, remaining traceable in particulate form to at least 50 km away from its source (Severmann et al., 2004), and even up to 4000 km in dissolved form (Resing et al., 2015). Considering the majority of microbial growth is predicted to occur in the neutrally buoyant portion of the plume (Reed et al., 2015), further efforts should be concentrated on sampling this portion of the plume.

In order to address this gap, water column and sediment samples from the Rainbow hydrothermal vent area were investigated during the TREASURE cruise. Geochemical and biological changes were explored vertically in the water column and horizontally along the neutrally buoyant plume using sector field inductively coupled plasma mass spectrometry (SF-ICP-MS) with high resolution (HR) to determine the (trace) metal and REE content of the SPM. Next generation sequencing methods were used to quantify

the microbial diversity in the pelagic system that was influenced by the hydrothermal plume. Whilst mechanic understanding of microbial and geochemical interactions in the plume would have required a different experimental setup, which was beyond the scope of the TREASURE project, this paper aims to contribute to knowledge of geochemical and biological heterogeneity in the surroundings of an SMS site, induced by the presence of an active hydrothermal plume, which should be taken into account in environmental impact assessments of SMS mining.

2 Material and methods

2.1 Study site

The Rainbow hydrothermal vent field (Fig. 1) is located on the Mid Atlantic Ridge (MAR) at 36°13.80 N, 33°54.14 W at approximately 2300 m water depth, southwest of the Azores. The vent field is located on the western flank on the non-volcanic Rainbow Ridge, in an offset between the South Alvin Mid Atlantic Ridge (AMAR) and AMAR segments of the MAR (German et al., 1996; Fouquet et al., 1998; Douville et al., 2002). It is located at the intersection between the non-transform fault system and the ridge faults (Charlou et al., 2002), making this vent field tectonically controlled. The vent field, which is approximately 100 by 250 m in size, is underlain by a basement composed of ultramafic rocks (Edmonds and German, 2004; Marques et al., 2006). The ultramafic setting of Rainbow is atypical for the region, which is dominated by basalt hosted vent systems (Douville et al., 2002). Due to serpentinization reactions during the circulation of the hydrothermal fluid in the peridotite basement rocks, the Rainbow vent field produced plumes particularly enriched in transition metals (notably Fe, Mn and Cu) and REEs (Douville et al., 2002; Findlay et al., 2015). On the contrary the plumes are depleted in hydrogen sulfides (Charlou et al., 2002; Douville et al., 2002), resulting in relatively high metal/sulfide ratios. Consequently, the chimneys and the SMS deposits of the Rainbow hydrothermal field are enriched in Cu, Zn, Co and Ni when compared to vent systems with a basaltic host rock (Charlou et al., 2002).

The vent field consists of 10 active, high temperature (365 °C) black smokers and emits an extensive plume with a distinct chemical composition compared to the ambient seawater (Severmann et al., 2004).

The plume is considered the largest and widest spreading in the region (German et al., 1996), rising up to 200 m above its source and traceable over at least 50 kilometres (Severmann et al., 2004). Controlled by the local hydrodynamic regime and topography (Thurnherr and Richards, 2001; Thurnherr et al., 2002), the neutrally buoyant plume moves predominantly to the north and east around the Rainbow Ridge with an average current speed of 5-6 cm s^{-1} and continues in a northward direction along the southern and eastern side of the rift valley of the AMAR segments (Edmonds and German, 2004). Characteristics and behaviour of the Rainbow plume are relatively well-studied which make the Rainbow vent field a suitable site to study neutrally buoyant plumes.

2.2 Water column and sediment sampling

Water samples and sediment cores were collected along the path of the plume during RV *Pelagia* cruise 64PE398 in April 2015. Five putatively distinct biotopes were sampled: (i) above plume (1000 m water depth), (ii) plume, (iii) below plume (10 metres above bottom), (iv) near-bottom water and (v) sediment.

Using CTD casts with a Seabird 911 CTD-Rosette system, the plume was traced in real time using turbidity as an indicator, measured in NTU with a WETLabs turbidity sensor. Other variables measured included temperature (°C), salinity, density (σ-θ, kg m^{-3}), dissolved oxygen (ml L^{-1}) and chlorophyll (µg L^{-1}). At five stations, continuous yoyo CTD-casts were taken over the course of 12 hours, to study the temporal changes of the hydrothermal plume.

A total of 41 water samples were collected using 12 L Niskin bottles from eleven downstream stations, two distal downstream stations and three upstream stations. Once the CTD was back on deck, three distinct water samples were immediately taken for suspended particulate matter (SPM), trace metals, and the microbial community.

Depths for sampling SPM were chosen to comprise the largest variation in turbidity measured by the WETLabs turbidity sensor in a vertical profile so that the sensor could be reliably calibrated and readings converted to mg L^{-1}. If possible, trace metal and microbial community samples were taken at the same stations and/or same depth.

Sediment and near-bottom water samples were collected with a NIOZ designed box corer of 50 cm diameter equipped with a top valve to prevent flushing, subsequently trapping near-bottom water (van Bleijswijk et al., 2015). In total eight cores were collected (Table 1). Due to unsuitable coring substrates, CTD locations and coring sites did not always follow the same track. Box cores were taken on the eastern part of the Rainbow Ridge, continuing in the basin east of the ridge, while two cores were taken on the north-western flank of the ridge, following the path of the plume.

2.3 Suspended particulate matter analysis

From each 12 L Niskin bottle, two 5 L subsamples were collected to determine the concentration of SPM. The subsamples were filtered on board over pre-weighed 0.4 µm polycarbonate filters. The filters were rinsed with ~10 ml of Milli-Q water to remove salt, while still applying under pressure, and subsequently stored at -20 °C on board. In the laboratory, the filters were freeze dried and then weighed in duplo, or in triplo if the difference between the first two measurements was more than 0.03 mg. To yield SPM concentrations, the net dry weight of the SPM collected on the filters (average of 0.25 mg), corrected by the average weight change of all blank filters (0.04 mg), was divided by the volume of filtered seawater (5 L). Subsequently, the filters were examined using a Hitachi TM3000 table-top scanning electron microscope (SEM) connected to an energy-dispersive spectroscopy (EDS)-detector to visualize content of the SPM and to qualitatively analyse the chemical composition. The SEM was operated under an acceleration voltage of 15 kV and a filament current of 1850 mA.

2.4 Chemical analysis

For analysis of major and trace metals present in particulate form in and around the hydrothermal plume, water samples were filtered on board over acid-cleaned 0.45 µm polysulfone filters directly from the Niskin bottle at ambient temperature while applying under pressure. A water barrel in between the filtration holder and pump allowed for volume measurements of filtered water. The filters were subsequently stored at -20 °C until further examination. Filters were dried in the laboratory in an Interflow

laminar flow bench at room temperature prior to analysis. Subsequently, the filters were placed in acid-cleaned Teflon vials and were subjected to a total digestion method. For this purpose a mixture of 6.5 ml HNO_3 (ultrapure)/HF (suprapure) (10:1) solution, 1 ml HCl (ultrapure) and 1 ml $HClO_4$ (ultrapure) was added to the vials, after which the vials were covered and placed in an Analab hotblock for 48 hours at 125 °C. After the filters were completely dissolved, the covers were taken off from the vials and the vials were left for 24 hours in order to evaporate the acids. Finally, the residue was taken up again in 10 ml 1M ultra grade HNO_3, pre-spiked with 5 ppb scandium and 5 ppb rhodium as internal standards. Furthermore, ten procedural blanks were performed. Half of them were empty acid-cleaned Teflon vials, the other five contained an acid-cleaned blank filter in order to correct for the dissolved filters. These blanks were subjected to the same total digestion method as described above. A SF-ICP-MS (Thermo Element II) at the Royal Netherlands Institute for Sea Research (NIOZ) was used to analyse the concentrations of major- and trace metals, as well as REEs. The concentrations were calculated using external calibration lines made from a multi stock solution, which was prepared by mixing Fluka TraceCert standards for ICP. Rh was used as an internal standard for all elements. The machine drift was measured before, half-way and after each series of samples and was monitored by using an external drift solution. Precision (relative standard deviation (RSD)) of these analyses was generally <2 % for major- and trace metals, apart from ^{115}In where the RSD values generally are between 4 % and 8 %, with maximum values going up to 12.48 %. For REEs, the RSD values were generally <3 %, apart from a few measurements where RSD values reached maximums up to 12.48 %. The accuracy could not be determined as no certified reference material was analysed.. A blank correction was applied to the sample data by subtracting average values measured for five dissolved blank filters, which, for the majority of the measured elements accounted for less than 10 % of the sample values. Subsequently the data was recalculated to account for the dilution of the samples during the total digestion and the amount of seawater that was filtered to yield the true concentration of each element.

2.5 Microbial community

Three distinct samples of 2 L of water were collected from three different Niskin bottles for Next Generation Sequencing (NGS). The water was filtered immediately after collection through a 0.2 µm polycarbonate filter (Nuclepore) facilitated by a vacuum of 0.2 bar, in a climate controlled room at 4 °C to limit DNA degradation. From the box cores >0.25 grams of surface sediment were scraped off with a sterilised spatula, whilst 1.5 L of overlying (near-bottom) water was filtered as above. Filters were stored in a 2 ml cryo-vial and all samples were stored at -80 °C on board.

DNA was extracted using a Power Soil DNA Isolation Kit (MoBio, now Qiagen) according to the manufacturer's protocol. Each DNA extract concentration was quantified using a Qubit 3.0 fluorimeter (Qiagen, Inc.) and stored at -20 °C before amplification. Extracts were combined with Phusion Taq (Thermo Scientific), High Fidelity Phusion polymerase buffer and universal primers to amplify the V4 region of 16 S rDNA of bacteria and archaea (Table 2), with unique molecular identifier (MID) combinations to identify the different samples. All negative controls from all PCR series were labelled with the same unique MID. The PCR settings were as follows: 30s at 98 °C, 29 cycles (10s at 98 °C, 20s at 53 °C, 30s at 72 °C) and 7 minutes at 72 °C. Four and three samples were re-run at 30 and 32 cycles, respectively, in order to yield enough product. Each sample was subjected to the polymerase chain reaction (PCR) protocol in triplicate and processed independently to avoid bias. 5 µl of product was used to screen the products on an agarose gel. The remaining 25 µl of each triplicate was pooled to evenly distribute the DNA, split into two slots and run on a 2 % agarose gel at 75 volts for 50 minutes. Sybergold stain was applied post run for 20-30 minutes before cutting the 380 bp bands out with a sterilised scalpel over a blue light to avoid UV damage. The two bands of mixed triplicates were pooled, purified using the Qiaquick Gel Extraction Kit (Qiagen, Inc.) and quantified with a Qubit™ 3.0 fluorometer (Qiagen, Inc.). Samples were pooled in equimolar quantities together with blank PCR controls. The pooled sample was concentrated using MinElute™ PCR Purification columns (Qiagen Inc.) as described by the manufacturer and sent to Macrogen (South Korea) for sequencing. Sequencing was undertaken with a Roches GS FLX instrument using Titanium chemistry on a one-eight region gasket and Roche GS FLX instruments. Sequence processing was undertaken as described by van Bleijswijk et al. (2015), using a QIIME pipeline.

Sequences shorter than 250 bases and average Q scores below 25 were removed. The OTU sequences (>98 % similarity) were classified (>93 % similarity) based on a recent SILVA SSU database (release 132; Yilmaz et al. 2014). Single reads were excluded and all data were standardised to remove any disproportionate sampling bias.

2.6 Statistics

Unconstrained ordination techniques were utilised to distinguish biotopes and general community patterns. Non-metric Multi-Dimensional Scaling plots (NMDS) were created based upon Bray-Curtis similarity matrices of square root transformed microbial community assemblages. Group average clustering was also utilised in order to quantify similarities between the samples. ANalysis Of SIMilarities (ANOSIM) was subsequently used to statistically test community distinctions based upon presumed biotopes (sediment, near-bottom water, below plume water, plume water and above plume water). In addition, all water column samples were plotted in separate NMDS plots to observe patterns in greater detail. Physical properties of all water samples (station, depth, turbidity and location) were depicted in a NMDS plot to observe sample similarities. These environmental data were normalised and Euclidean distance was used to create a similarity matrix. The relationship between Fe and turbidity was tested with a linear regression analysis. Trace metals and REEs were normalised to Fe, since it is the primary particle-forming element at all stages of plume dispersion, giving insight in the chemical behaviour. All multivariate statistics were undertaken in Primer™ V6 (Clarke and Gorley, 2006).

Shannon-Wiener index (loge) was calculated as a diversity measure. Biodiversity differences between biotopes were tested with the non-parametric test Kruskal-Wallis with pairwise comparisons as the data did not meet normality or homogeneity assumptions, even after transformation. These statistical tests were undertaken in SPSS.

A SIMililarities PERcentage analysis (SIMPER in Primer v6) was applied on the microbial class level with a cut off for low contributions at 90 % based on Bray-Curtis similarity matrix to characterise the community composition based on groups contributing to intra biotope similarities. Relationships between

environmental variables and microbial classes as a percentage of each composition within the plume, were tested with Pearson correlation and hierarchical clustering to identify broad response groups.

3 Results

3.1 Water column characteristics

Temperature, salinity and density plots indicated that the water column at each location had similar physical traits, whereby three main different water masses could be distinguished (Fig. S1). The surface Eastern North Atlantic Central Water (ENACW) was characterised by a temperature, salinity and density at the surface of 18 °C, 36.4 and 26.2 kg m^{-3} to 11 °C, 35.5 and 27.2 kg m^{-3} at the bottom of the water mass. The underlying Mediterranean Outflow Water (MOW) was characterised by a temperature of 7.5-11 °C, a salinity of 35.4-35.5 and a density of 27.2-27.75 kg m^{-3}. The North Atlantic Deep Water (NADW) was characterised by temperatures ranging from 4 to 7.5 °C, salinity of 35.0 to 35.4 and a density of 27.75 to 27.825 kg m^{-3} (Emery and Meincke, 1986). The neutrally buoyant plume was centred around the 27.82 kg m^{-3} isopycnal, as illustrated in Figures 2 and 3.

3.2 Turbidity and plume dispersion

Against a background of non-plume influenced waters, as found in the CTD casts, with typical concentrations of SPM of 0.04 mg L^{-1} (0.015 NTU), the neutrally buoyant plume stands out as a layer with distinctly higher turbidity values (i.e. higher SPM concentrations) consistently present in the depth interval of 1750 – 2400 m at stations located north and east of Rainbow (Fig. 2). Except where this turbid water layer was found impinging the seabed, relatively clear waters separated the turbid layer from the underlying seabed.

At downstream stations, a consistent trend of decreasing turbidity and increasing vertical dispersion was noted. At station 27, 3.5 km north of Rainbow, maximum turbidity in the core of the plume was 0.15 NTU (0.09 mg L^{-1}) and plume thickness was about 105 m, whilst at station 46, 15.2 km east of Rainbow,

maximum turbidity was only 0.08 NTU (0.06 mg L^{-1}) and plume thickness was 275 m. Away from the main plume path, station 47 and 49 (13.8 and 16.5 km from Rainbow, respectively) showed a diluted signature similar to that observed at the most distal stations along the main plume path. Despite being most proximal to Rainbow, station 16, located 1.0 km downstream of Rainbow, showed a relative low turbidity of 0.015 NTU (0.04 mg L^{-1}). Since the plume is more constrained closer to the source, the main body of the narrower plume could have been missed with the CTD. Stations upstream of the vent site (station 13 and 28, 4.2 and 7.5 km southwest of Rainbow respectively and station 40, 3.6 southeast of Rainbow) displayed low turbidity values, ranging between 0.01 and 0.02 NTU (0.04 mg L^{-1}) (Fig. S2).

The CTD profiles from stations 42 and 49 (4.9 and 16.5 km north of Rainbow respectively) both displayed highest turbidity in the lower hundreds of metres above the seafloor, with instances of seafloor contact during time of sampling. Therefore no samples could be taken below the plume at these stations. The assumption that the plume is subject to vertical movement is supported by observations made during 12-hour CTD yoyo casts carried out at station 27 (Fig. 3). Along with vertical displacements of the 27.82 kg m^{-3} isopycnal on the order of 150 m, likely reflecting internal tidal motions, the hydrothermal plume was found to also move up and down, at times touching the seafloor.

3.3 Enrichment of (trace) metals compared to the ambient seawater

NMDS ordination (Fig. 4) based on Euclidean distance resemblance of normalised element/Fe molar ratio data of all collected water samples (2D stress = 0.03), revealed a clear distinction of the different samples. Most outstanding are the samples from above plume waters, indicating that the chemical composition is different from the other samples.

The remaining samples showed less variation, nonetheless the samples collected from below the plume and the samples collected away from the main path of the plume can be distinguished. This shows that the hydrothermal plume can be characterised by its chemical composition. When comparing samples taken in the turbidity maximum of the plume to the above plume water samples taken at 1000 m water depth it is found that Fe, Cu, P, V and Pb are enriched by factors of ~80, ~90, ~17, ~52 and ~25

313 respectively. Elements with a more moderate degree of enrichment are Co, Mn, Zn, Al and Ni, with
314 enrichment factors of ~8.0, ~2.5, ~10.3, ~1.4 and ~1.6, respectively. The REEs were enriched by a factor
315 of 5 to 40 relative to the clear water. U, Ti and Ca are slightly enriched at turbidity maxima, by factors of
316 ~1.3, ~1.6 and ~1.2, respectively. In and Sn are depleted compared to the above plume water.

317

318 **3.4 Geochemical gradients within the hydrothermal plume**

319 Within the hydrothermal plume, geochemical evolution is found as the plume disperses. Visual
320 examination of the samples with the SEM coupled with chemical analysis performed with the EDS-
321 detector revealed that the SPM within the plume close to the Rainbow hydrothermal vent at station 32
322 (2.9 km north of Rainbow) mainly consisted of Fe-sulfides. In the plume samples further downstream, Fe
323 is mainly present as Fe-oxides, Fe-hydroxides or bound in alumino-silicates.

324 Chemical examination of the samples showed gradients in the element/Fe molar ratios along the path of
325 the plume as well as off the main path of the plume at upstream and the most distal downstream stations.
326 Since the Fe concentration is linearly related to the turbidity (Fig. 5) (R^2 = 0.9356, $P < 2.2*10^{-16}$),
327 normalisation to Fe reveals relative enrichments or depletion of common elements. The chalcophile
328 elements Co, Cu and Zn show a partly-linear relation steepening with increasing Fe concentration (Fig.
329 6A for Cu), indicating that the element/Fe molar ratios are elevated close to the source but decrease
330 towards the more distal sites (Fig. 7A). One exception is the Zn/Fe molar ratio, which is elevated at station
331 37, 39 and 44. Furthermore, a high Zn/Fe molar ratio is observed at upstream station 40. The oxyanions
332 P and V are linearly related to Fe (Fig. 6B for V), and shows varying element/Fe molar ratios without a
333 clear trend of increasing or decreasing ratios, both upstream and downstream of Rainbow (Fig. 7B). The
334 REEs show a partly-linear relation levelling-off with increasing iron concentrations (Fig. 6C for Y).
335 Within the plume this is displayed as increasing element/Fe molar ratios towards station 44, with station
336 42 as an exception, followed by slightly decreasing molar ratios from station 44 onwards (Fig. 7C). The
337 Ca/Fe molar ratios ranged between 0 and 15 for most of the downstream stations, apart from the stations
338 further downstream (47 and 49), which displayed slightly higher Ca/Fe molar ratios. Upstream station 28
339 had a Ca/Fe molar ratio similar to those found at station 47 and 49 and upstream station 40 was found to

have a significantly higher Ca/Fe molar ratio (Fig. 7E). Other analysed elements, Mn, Al, Ni, In, Pb, Sn, Ti and U showed no clear relationship with the Fe concentration (Fig. 6D for Sn). However, within the plume it was found that the Mn/Fe molar ratio is lower than at the upstream stations or the more distal downstream stations.

3.5 Microbial assemblages in water column biotopes

Samples from sediment, near-bottom water and no plume water contained microbial communities which clustered distinctly from each other and from plume, below plume and above plume communities (Fig. 8). In particular, sediment, near-bottom water and no plume (station 13) samples have communities that are very dissimilar from the overlying water column samples. Sediment samples appeared to cluster in a straight line suggesting some sort of gradient of similarity along the ordination axis, though no apparent patterns were observed when independently plotted. The near-bottom water samples were relatively dispersed in the NMDS plot suggesting a more variable community. Samples taken at the upstream station 13 from below plume and plume depths showed no similarity with samples from corresponding depths in the other stations, whilst the above plume community at this station is consistent with that of other stations. In general, plume and below plume communities were more similar nearer to the vent source, with stations further downstream displaying greater dissimilarity (Fig. 9, Fig. S3).

Group average cluster analysis showed high level of dissimilarity, i.e. large community variation, between and within biotopes. ANOSIM revealed all putative biotopes that were sampled had distinct communities (Global $R = 0.738$; $p = 0.001$; 999 permutations), except for plume and below plume samples which could not be distinguished statistically (Global $R = -0.091$; $P = 0.861$). The two seemingly unique samples from station 13 also tested significantly distinct, but with a low number of permutations (<999) due to low replication (n=2).

3.6 Univariate biodiversity

Plume and below plume samples were less diverse than sediment samples, whilst diversity in the plume was lower than in near-bottom water samples (Kruskal-Wallis: $\chi 2$ (4) = 36.127, P < 0.01). In general, plume diversity was low (Fig. 10), but further differences were not statistically significant, likely due to limited replication and intra biotope variation.

The plume microbial community at sites upstream of Rainbow and at the immediate downstream sites (stations 28, 13, 16 and 27) showed similar and relatively high biodiversity (>4.5) (Fig 11). Plume biodiversity at the sites further away from Rainbow gradually decreased until station 46, which displayed the lowest Shannon-Wiener index value of 2.4. Distant stations 47 and 49, showed biodiversity rising to a more moderate index value around 3.5.

3.7 Species composition

Results of the SIMPER analyses showing the contributions of taxa composition to similarities within biotopes (Table 3), mirrored the NMDS and ANOSIM results whereby the similarity of community composition in each biotope was dominated by a different makeup of the microbial community. The Archaeal class Nitrososphaeria (Marine group 1 archaea) contributed the most to similarity within the above and below plume water communities, while also being very common in all water samples. Alphaproteobacteria, Gammaproteobacteria and Deltaproteobacteria also constituted as a large makeup of all biotopes in the area. The class Epsilonproteobacteria were rare in above plume samples, and only contributed <2 % to near-bottom water communities. By contrast, Epsilonproteobacteria were dominant in plume water samples (accounting for >35 % of the community), and were the fifth most dominant taxon in below plume water samples contributing 8.9 % of the community.

Epsilonproteobacteria accounted for about 20 % of the plume community at stations near the vent. Beyond the near vent stations, an increase in relative abundance of Epsilonproteobacteria with distance from vent was observed, accounting for 64 % of the community at the distant station 46 (Fig. 12). Alphaproteobacteria, Deltaproteobacteria and Gammaproteobacteria appeared to become less dominant

391 with distance from the plume source (Fig. 12). The communities at distant stations 47 and 49 were less
392 dominated by Epsilonproteobacteria (around 40 %). Below plume communities were dominated mostly
393 by Nitrososphaeria (Marine group 1 Archaea) whereby Nitrosphaeria became more dominant with
394 distance from the plume source likewise as the Epsilonproteobacteria in the plume. Correlations between
395 environmental variables (elemental chemistry and physical properties) and all microbial classes observed
396 in the plume were evident and appeared class specific (Fig. S4). The hierarchical clustering revealed eight
397 broad response groups, which displayed different relationships with the environmental variables.

398

399 # 4 Discussion

400 Using a multidisciplinary approach in which physical, geochemical and ecological data were collected
401 from the Rainbow vent neutrally buoyant plume and its underlying sediment, we aimed to expand
402 knowledge and characteristics of the background (i.e. before impact) state of a hydrothermal vent. Such
403 knowledge is deemed essential to be able to assess (potential) impacts of future deep-sea SMS mining, as
404 it may help in characterising the behaviour of the dilute distal part of chemically enriched mining plumes.
405 We found geochemical and microbial differences between the above plume, plume, below plume and no-
406 plume water and in addition, pertinent chemical and biological gradients within the extensive Rainbow
407 hydrothermal vent plume were evident.

408

409 ## 4.1 Physical constraints of plume location and behaviour

410 The plume was observed within the NADW mass, constrained to an isopycnal density envelope of 27.82
411 kg m^{-3} (Fig. 2 and 3). The apparent continuity of this turbid water layer, especially to the NE of the
412 Rainbow field, and lack of similarly turbid waters in the bottom waters below the plume, link the plume
413 to Rainbow and preclude local sediment resuspension as origin. Using turbidity measurements and
414 presumed plume path, we traced the plume up to 25 km away from the vent source. This is within the
415 range mentioned by German et al. (1998) who found that the Rainbow plume extends over 50 km, being
416 controlled by local hydrodynamics and topography. Unexpectedly, in the basin upstream of the Rainbow

vent field a turbidity peak at 1975 m water depth resembling a plume was observed as well (station 28), confounding our assumption of a clear water column at upstream stations and distant downstream stations. This suggests that the plume is distributed much further than previously observed by Thurnherr and Richards (2001) and German et al. (1998). This is exemplified by the local variation in microbial community composition of upstream stations (Fig. 12) and is supported by the relatively low Ca/Fe molar ratio at station 28 (Fig. 7), indicating hydrothermal influence. In addition, the observed variability of plume strength and vertical position (Fig. 3) indicate that local fluctuation in the current regime and tidal motions influence the plumes behaviour. This dynamic behaviour has implications for surveys designs and should be considered when monitoring natural and man-made plumes, such as mining-related plumes. Prior insight into plume extension and behaviour is required for the identification of adequate control sites and for tracking of plume evolution in future impact studies.

4.2 Plumes influence on the water column chemical and microbial make-up

The neutrally buoyant plume introduced pelagic heterogeneity in terms of chemical and microbial composition, which is supported by the vertical classification of the different biotopes. The neutrally buoyant plume was evidently enriched in metals and REEs compared to overlying clear water. Element concentrations were found to be in line with those found by German et al. (1991) and Edmond et al. (1995) and Edmonds and German (2004) who have studied the Trans-Atlantic Geotraverse (TAG) hydrothermal plume and the Rainbow hydrothermal plume, respectively. Our chemical results from Rainbow also match with those of Ludford et al. (1996), who have studied vent fluid samples from the TAG, Mid-Atlantic Ridge at Kane (MARK), Lucky Strike and Broken Spur vent sites, i.e. element concentrations were found to be in the same order of magnitude (Table S2).

The distinctive chemical composition of the plume samples (e.g. metal concentrations) affects chemolithoautotrophic microbial growth within the plume as indicated by the typical microbial community in plume samples. We observed a clear and consistent separation between communities in the plume and those in above plume samples. The influence of MOW on the above plume community could also play a role, as water masses can harbour different microbial communities (Agogue et al., 2011).

However, the palpable presence of a plume in the turbidity data with supporting chemical measurements, and the occurrence of vent associated Epsilonproteobacteria (Olins et al., 2017; Djurhuus et al., 2017) and other vent associated groups such as the Gammaproteobacteria clade SUP05 (Sunamura et al., 2004), point to a unique chemical environment. Here chemosynthetic communities flourish and give rise to independent biotopes in the neutrally buoyant plume kilometres downstream of the vent site.

Below plume communities were not distinct from the plume biotope, although instead of Epsilonproteobacteria, the ubiquitous class Nitrososphaeria was the most dominant group, reflecting some similarities with above plume seawater communities. Similarities between plume and proximal habitat communities have also been observed by Olins et al. (2017), whereby intra-field (defined as within vent field between diffuse flows) and diffuse flow microbial communities were alike. In our study, similarities between plume and below plume are likely derived by precipitation of mineral and microbial aggregates dragging plume microbes deeper below the plume as suggested by Dick et al. (2013). In addition, internal wave induced turbulence causes vertical mixing along the slope of the Rainbow Ridge (van Haren et al., 2017), which may cause the plume and associated communities near the vent field to mix with ambient water communities leading to assemblage similarities. This indicates the plume and associated microbial processes could have a larger vertical footprint than previously observed, supporting suggestions by Olins et al., (2017) that proximal non-plume habitats have been overlooked. Interestingly, near-bottom water (and sediment) community assemblages were distinct from the below plume and other water column communities. This could imply: 1) that there is little ”fall out” from the plume at distance from the vent which is in agreement with sediment trap observations by Khripounoff et al. (2001), 2) plume specific bacteria die off due to lack of energy sources and DNA degrades before reaching the seafloor, 3) microbes are more abundant in the near-bottom waters, either naturally or through mechanical disturbance resuspending sediment during the coring process, outnumbering groups that have been mixed in from overlaying water. Despite the presence of a plume and precipitation, a difference between the sea floor and the water column biotopes is present, consistent with global broad scale non-vent benthic-pelagic patterns (Zinger et al., 2011). According to Khripounoff et al. (2001) particulate fall-out from the Rainbow plume is spatially very limited. This implies that the extended chemical imprint on the sediment (reported by Cave et al. (2002), Chavagnac et al. (2005), and this study), is likely to have formed when

the plume is in direct contact with the sediment during its vertical tidal migration. As the plume rises again, the associated distinct communities apparently resume dominance in the near-bottom water. Though Epsilonproteobacteria have been detected in Rainbow vent sediments comprising over 5 % of the sediment community (Lopez-Garcia et al., 2003), very few reads of this group in sediment samples were present in our study, probably as our coring samples were collected kms away from the venting site. Cave et al. (2002), observed chemical evolution of sediment composition with distance from source, thus we infer a relationship between the sediment dwelling Epsilonproteobacteria with nearby plume precipitates, such as Cu and presumed precipitates Zn and Cd (Trocine and Trefry, 1988). Additionally, extracellular DNA degradation rate can be 7 to 100 times higher in sediment than in the water column (Dell'Anno and Corinaldesi, 2004). Therefore, although our results suggest no microbial plume community imprint on the sediment, we cannot rule out short lived episodic community changes when the plume is in contact with the sediment.

4.3 Geochemical gradients within the hydrothermal plume

Analysis of SPM in water samples taken along the flow path of the plume, as well as off the flow path, showed conspicuous trends of elements, reflecting the chemical evolution of the plume as it drifts away from its hydrothermal source.

The chalcophile elements (Cu, Co and Zn) were found to have the highest element/Fe molar ratios closest to the vent site, indicating either rapid removal from the hydrothermal plume or removal from the solid phase as the plume drifts away from the vent site. Using SEM-EDS, it was demonstrated that at the proximal downstream stations mainly Fe-sulfides were found, whereas Fe-(oxyhydr)oxides were found further downstream. This suggests that chalcophile elements are mainly present in the form of sulfide mineral particles at the proximal stations, which are entrained in the flow of hydrothermal water emanating from the Rainbow vents and subsequently rapidly lost by settling from the plume in sulfide-bearing phases, while a large portion of Fe remains in suspension (Cave et al., 2002; Edmonds and German, 2004), consistent with decreasing concentrations of Cu, Zn and Co in sediment recovered from the Rainbow area with increasing distance to the vent site (Cave et al., 2002).

The oxyanions (V and P) showed slightly varying element/Fe molar ratios with increasing distance away from Rainbow, suggesting co-precipitation with Fe as oxyhydroxides (Edmonds and German, 2004). No additional uptake of these elements was observed with increasing distance from the vent field (German et al., 1991), since these elements are scavenged initially in significant amounts during the buoyant plume phase (Cave et al., 2002).

The trend shown by Mn/Fe molar ratios can be attributed to the slower oxidation kinetics of Mn (Cave et al., 2002). It takes longer for reduced Mn to be oxidised than it would for Fe, resulting in an increase in particulate Mn with increasing distance from the Rainbow hydrothermal vent field, which subsequently settles out from the plume as Mn-oxyhydroxides (Cave et al., 2002).

The observed positive relationship between the REEs and Fe is indicative of continuous scavenging of these elements from the ambient seawater onto Fe-oxyhydroxides (Edmonds and German, 2004; Chavagnac et al., 2005; Caetano et al., 2013). Therefore, the highest element/Fe molar ratios were observed away from the Rainbow hydrothermal vent site, where Fe-(oxyhydr)oxides are dominant more distal to the vent site.

The Ca/Fe molar ratios vary between 0 and 15 for the stations downstream of the Rainbow hydrothermal vent, but are higher at the distant downstream station 47 and 49 and upstream stations 28 and 40. Especially at station 40, located on the Rainbow Ridge, the Ca/Fe molar ratio is significantly higher than at the other stations. This is in line with observations by Khripounoff et al. (2001) and Cave et al. (2002) who also found that the relative Ca concentration in settling particles and the sediments is lower close the Rainbow vent field and increases as the Fe concentration decreases when the plume disperses. Since Ca is naturally present in high abundances in pelagic skeletal carbonate which rains down from the overlying water column and Fe is mainly present as a hydrothermal component the Ca/Fe molar ratio could be an indicator for the extent of the hydrothermal influence. The high molar ratio at station 40 would then suggest that this station is hardly or not at all influenced by the hydrothermal plume as the natural abundance of particulate iron is low (e.g. Michard et al., 1984 and this study), whereas station 28, 47 and 49 are, as expected, influenced in more moderate degrees compared with the stations directly downstream of Rainbow.

4.4 Microbial gradients within the hydrothermal plume

The microbial plume community composition and diversity altered with distance from the plume source, showcasing horizontal heterogeneity within the plume. Despite dilution, the vent associated group Epsilonproteobacteria (specifically the most common genus *Sulfurimonas*), appeared to dominate the community composition. This is likely due to its flexibility to exploit a range of electron donors and acceptors (Nakagawa et al., 2005), making them suitable inhabitants of dynamic environments (Huber et al., 2003). From the relative abundance data presented here it cannot be determined whether Epsilonproteobacteria dominate by rapid reproduction or if other groups decline in abundance. However, it is evident that Epsilonproteobacteria remain competitive or outcompete other competitors such as generalists Gammaproteobacteria that are often vent associated (i.e. SUP05). It is unlikely that this pattern is caused by entrainment of Epsilonproteobacteria from background seawater over time. This is based on the lack of significant presence of Epsilonproteobacteria in above plume water and at remote station 13, and reduced mixing that neutrally buoyant plumes generally experience (McCollom, 2000). This is further supported by the increasing uniqueness of the plume community with distance from the source, suggesting that mixing and entrainment between downstream biotopes is negligible.

The neutrally buoyant plume is likely too chemically enriched for non-adapted microbial taxa to thrive, and consequently are outcompeted by groups that can benefit from or tolerate the chemical nature of the plume. Therefore, it is likely that less specialised groups die out due to lack of appropriate resources and interspecies competition, as indicated by the decline in biodiversity with age of plume (distance) directly mirroring the increasing dominance of Epsilonproteobacteria, a group already known to influence diversity and community structures (Opatkiewicz et al., 2009; Sylvan et al., 2012). In addition, the decrease in concentration of particulate matter may influence microbial diversity (Huber et al., 2003). Temporal succession has been observed within plume environments by Sylvan et al., 2012 and Reed et al., 2015, driven by metabolic energy yield and concentration of the electron donors. These patterns may relate to ecological succession (Connell and Slaytor, 1977) within the plume with change in microbial communities resulting in a low diversity, climax plume community. At the distant stations 47 and 49, the community was less dominated by Epsilonproteobacteria and more diverse, indicating a gradual return to

what is possibly a non-plume influenced state of the microbial community. The wide range of correlations within and between microbial classes and water properties, i.e. ranging from chemical to physical variables (Fig. S4), indicates a complex array of community drivers within the plume.

In contrast to our results, Sheik et al. (2015) and Djurhuus et al. (2017), observed decreasing Epsilonproteobacteria abundance within hundreds of metres from the source in the rising, buoyant portion of plumes generated by Indian Ocean and South Pacific vents. Interestingly, in our results Epsilonproteobacteria were least dominant in the neutrally buoyant plume closest to the Rainbow vent site, which may indicate that entrainment of other microbial groups within the rising portion of the plume initially dilutes the contribution of Epsilonproteobacteria (possibly derived from near seafloor communities), whilst the competitive advantage of certain species from this group becomes only evident at a later stage as the plume drifts away from the source. However, Huber et al., 2003 suggested that Epsilonproteobacteria, thrive in hydrothermal fluid mixed with seawater due to lower temperature and great electron acceptor availability, suggesting greater habitat suitability away from the immediate venting orifice. Furthermore, it has been demonstrated that Epsilonproteobacteria (specifically *Sulfurimonas*) have higher dispersal capabilities than thermophilic vent associated microbial groups (Mino et al., 2017). A sampling design to follow the continuity of the plume from the buoyant to the neutrally buoyant portion would be a suitable approach to fully trace the evolution of the plume from the orifice to full dilution. However, the term full dilution is ambiguous as it is unknown exactly how far the plume influences the water properties and how far the plume associated bacteria will follow, adding water column microbial community heterogeneity beyond our study spatial extent.

4.5 Possible effects of SMS mining plumes

Mining of SMS deposits will create additional plumes generated by activities of mining vehicles (resuspension) and by the discharge of solids from the surface vessel (discharge plume). It is yet unknown how these plumes will affect the ecosystem at active and inactive hydrothermal vent sites. Our study showed the influence of a natural hydrothermal plume on the pelagic microbial and chemical composition

up to 25 km away from its source. Not unlikely, the dispersion of sediment and chemically reactive mineral material in the water column may cause similar or larger changes to the background state.

While large particles mobilised by mining are expected to stay close to the seafloor and settle out rapidly, smothering fauna in the immediate surroundings (Jones et al., 2018), smaller particles will disperse further, potentially invoking effects on a larger spatial scale. Modelling the behaviour of the discharge plume generated by the proposed Solwara 1 SMS mining has shown that these plumes can extend up to 10 km from the mining site, resulting in a deposit thickness of up to 50 cm within 1 km of the discharge site (Gwyther et al., 2008; Boschen et al., 2013). Apart from the physical impact that suspended fine-grained solids may have, especially on suspension feeders, the presence of chemically reactive material may give the mining plume a distinct chemical and microbial fingerprint, analogues to a certain context to what we observed in the natural plume.

The extent of the local impact of deep-sea mining will depend on the location where the mining takes place. At an active site like the Rainbow hydrothermal vent field, we showed that even in the distant plume (25 km away from Rainbow) hydrothermal plume microbiota dominate. When a mining discharge plume at an active hydrothermal vent field would be merged with the natural plume, the local effects might be minimal since microbial communities are already adapted to the metal-rich environments (Gwyther et al., 2008). However, a mining plume consisting of a dense suspension of bottom sediment and fine-grained metal sulfides is expected to support an altered microbial community in terms of abundance and composition, impacting the hydrothermal plume community. Moreover, the effects over larger spatial scales could be multiplied because of the increased export of electron donors by mining activities. Reed et al. (2015), who studied a hydrothermal plume in the Lau basin, have shown that the export of the chemolithoautotrophs from a plume increases with increasing availability of electron donors. Dispersion of chemolithoautotrophs is variable between groups depending on the energetics of their metabolisms, for example, methanotrophs which could disperse more than 50 km, are likely to disperse further than sulfur oxidisers (Reed et al., 2015). Increased export of microbial biomass from plumes may have impact on other marine systems which are hospitable to chemolithoautotrophs, such as oxygen minimum zones (Dick et al., 2013) and to higher trophic levels (Phillips, 2017). At inactive sites the effect

on the background fauna is also potentially large since these are not adapted to the heavy metal rich environments and the discharge plume could prove to be toxic to the fauna (Boschen et al., 2013), possibly affecting organisms at all levels of the food chain (Weaver et al., 2018). In addition, in case of multiple plumes at different depths due to stratification and vertical migration due to tidal regimes, the impacts may not be confined to a single depth band and may affect a large part of the water column, including other habitats, such as benthic habitats.

5 Conclusion

Our results demonstrate geochemically enriched plumes provide a dynamic habitat that is conducive to ecological changes in a short time span. Combining microbial and chemical analysis has proven to be a sensitive tool which enabled us to trace the hydrothermal plume up to 25 km downstream from the vent source and also upstream of the Rainbow vent site, implying that the influence of the hydrothermal vent on the surrounding environment may reach further than previously thought. The neutrally buoyant plume was chemically enriched which spawned a distinct microbial biotope dominated by vent associated species. As the plume aged and dispersed we observed alteration of the chemical composition and microbial community composition of the plume, showcasing a horizontal heterogeneous plume. Overall we have shown that a hydrothermal plume acts as a unique chemically enriched environment where distinct and variable microbial habitats are present. The plume heterogeneity and its dynamical behaviour would require extensive sampling in order to be able to assess the impacts and interferences by man-made mining plumes on the natural conditions.

Data availability

CTD data presented in this work, filter weights for SPM sampling, geochemical data of the (trace) metals and REEs, associated calculated enrichment factors and information on the blanks, drift measurements and detection limits of the SF-ICP-MS analyses are available in the NIOZ data portal (https://dataverse.nioz.nl/dataverse/doi under DOI 10.25850/nioz/7b.b.s) and will also be made available

in PANGAEA. Raw sequence data will be available via the European Nucleotide Archive (ENA) under accession number PRJEB36848, once the paper is published.

Author contribution

GD, HDS, and FM conceptualised the study and undertook data collection. SH and DP undertook sample processing and analysis with contributions from and under the supervision of FM, GD, GJR, HDS, JvB and HW. SH and DP wrote the manuscript with contributions from all co-authors.

Competing interests

The authors declare that they have no conflict of interest.

Acknowledgements

This study was carried out in the framework of the TREASURE (Towards Responsible ExtrAction of SUbmarine REsources) project, funded (grant number 13273) by the Applied and Engineering Sciences (AES) domain of the Netherlands Organisation for Scientific Research (NWO) and by partners from the Dutch maritime industry. Topsector Water, a collaborative effort of Dutch industry, academia and government, funded ship time. We thank Evaline van Weerlee for assistance in DNA extraction and Patrick Laan for assistance in the chemical analysis of the collected samples. We also thank the crew and captain of the RV *Pelagia*, as well as NIOZ technicians for their essential assistance during cruise 64PE398. We thank Valérie Chavagnac and anonymous reviewer 2 for reviewing the paper and their collective constructive feedback. SH received funding from the Blue Nodules project, EC grant agreement. 688785. DP is supported by the Natural Environmental Research Council [grant number NE/N012070/1]. HdS received funding from TREASURE. FM is supported financially by the Innovational Research Incentives Scheme of the Netherlands Organisation for Scientific Research (NWO-VIDI grant 016.161.360).

References

Agogue, H., Lamy, D., Neal, P. R., Sogin, M. L., and Herndl, G. J.: Water mass-specificity of bacterial communities in the North Atlantic revealed by massively parallel sequencing, Mol Ecol, 20, 258-274, https://doi.org/10.1111/j.1365-294X.2010.04932.x , 2011.

Anantharaman, K., Breier, J. A., and Dick, G. J.: Metagenomic resolution of microbial functions in deep-sea hydrothermal plumes across the Eastern Lau Spreading Center, Isme J, 10, 225-239, https://doi.org/10.1038/ismej.2015.81, 2016.

Boschen, R. E., Rowden, A. A., Clark, M. R., and Gardner, J. P. A.: Mining of deep-sea seafloor massive sulfides: A review of the deposits, their benthic communities, impacts from mining, regulatory frameworks and management strategies, Ocean Coast Manage, 84, 54-67, https://doi.org/10.1016/j.ocecoaman.2013.07.005, 2013.

Breier, J. A., Toner, B. M., Fakra, S. C., Marcus, M. A., White, S. N., Thurnherr, A. M., & German, C. R.: Sulfur, sulfides, oxides and organic matter aggregated in submarine hydrothermal plumes at 9 50′ N East Pacific Rise. Geochim. Cosmochim. Acta, 88, 216-236, https://doi.org/10.1016/j.gca.2012.04.003, 2012.

Caetano, M., Vale, C., Anes, B., Raimundo, J., Drago, T., Schimdt, S., Nogueira, M., Oliveira, A., and Prego, R.: The Condor seamount at Mid-Atlantic Ridge as a supplementary source of trace and rare earth elements to the sediments, Deep-Sea Res Pt Ii, 98, 24-37, https://doi.org/10.1016/j.dsr2.2013.01.009, 2013.

Cave, R. R., German, C. R., Thomson, J., and Nesbitt, R. W.: Fluxes to sediments underlying the Rainbow hydrothermal plume at 36 degrees 14' N on the Mid-Atlantic Ridge, Geochim Cosmochim Ac, 66, 1905-1923, https://doi.org/10.1016/S0016-7037(02)00823-2, 2002.

Cerqueira, T., Barroso, C., Froufe, H., Egas, C., and Bettencourt, R.: Metagenomic Signatures of Microbial Communities in Deep-Sea Hydrothermal Sediments of Azores Vent Fields, Microb Ecol, 76, 387-403, https://doi.org/10.1007/s00248-018-1144-x, 2018.

Charlou, J. L., Donval, J. P., Fouquet, Y., Jean-Baptiste, P., and Holm, N.: Geochemistry of high H_2 and CH_4 vent fluids issuing from ultramafic rocks at the Rainbow hydrothermal field (36 degrees 14' N, MAR), Chem Geol, 191, 345-359, https://doi.org/10.1016/S0009-2541(02)00134-1, 2002.

Chavagnac, V., German, C. R., Milton, J. A., and Palmer, M. R.: Sources of REE in sediment cores from the Rainbow vent site (36 degrees 14' N, MAR), Chem Geol, 216, 329-352, https://doi.org/10.1016/S0009-2541(02)00134-1, 2005.

Clarke, K. R., Gorley, R. N.: PRIMER v6: User Manual/Tutorial (Plymouth Routines in Multivariate Ecological Research), PRIMER-E, Plymouth, 2006

Collins, P. C., Croot, P., Carlsson, J., Colaço, A., Grehan, A., Hyeong, K., Kennedy, R., Mohn, C., Smith, S., and Yamamoto, H.: A primer for the Environmental Impact Assessment of mining at seafloor massive sulfide deposits, Mar Policy, 42, 198-209, https://doi.org/10.1016/j.marpol.2013.01.020, 2013.

Connell, J. H., and Slayter, R. O.: Mechanisms of Succession in Natural Communities and Their Role in Community Stability and Organization, Am Nat, 111, 1119-1144, https://doi.org/10.1086/283241, 1977.

Cowen, J. P., and Bruland, K. W.: Metal Deposits Associated with Bacteria - Implications for Fe and Mn Marine Biogeochemistry, Deep-Sea Res, 32, 253-&, https://doi.org/10.1016/0198-0149(85)90078-0, 1985.

Cowen, J. P., Massoth, G. J., and Feely, R. A.: Scavenging Rates of Dissolved Manganese in a Hydrothermal Vent Plume, Deep-Sea Res, 37, 1619-1637, https://doi.org/10.1016/0198-0149(90)90065-4, 1990.

Dell'Anno, A., and Corinaldesi, C.: Degradation and turnover of extracellular DNA in marine sediments: Ecological and methodological considerations, Appl Environ Microb, 70, 4384-4386, https://doi.org/10.1128/AEM.70.7.4384–4386.2004, 2004.

Dick, G. J., Clement, B. G., Webb, S. M., Fodrie, F. J., Bargar, J. R., and Tebo, B. M.: Enzymatic microbial Mn(II) oxidation and Mn biooxide production in the Guaymas Basin deep-sea hydrothermal plume, Geochim Cosmochim Ac, 73, 6517-6530, https://doi.org/10.1016/j.gca.2009.07.039, 2009.

Dick, G. J., and Tebo, B. M.: Microbial diversity and biogeochemistry of the Guaymas Basin deep-sea hydrothermal plume, Environ Microbiol, 12, 1334-1347, https://doi.org/10.1111/j.1462-2920.2010.02177.x, 2010.

Dick, G. J., Anantharaman, K., Baker, B. J., Li, M., Reed, D. C., and Sheik, C. S.: The microbiology of deep-sea hydrothermal vent plumes: ecological and biogeographic linkages to seafloor and water column habitats, Front Microbiol, 4, https://doi.org/10.3389/fmicb.2013.00124, 2013.

Djurhuus, A., Mikalsen, S. O., Giebel, H. A., and Rogers, A. D.: Cutting through the smoke: the diversity of microorganisms in deep-sea hydrothermal plumes, Royal Society Open Science, 4, https://doi.org/10.1098/rsos.160829, 2017.

Douville, E., Charlou, J. L., Oelkers, E. H., Bienvenu, P., Colon, C. F. J., Donval, J. P., Fouquet, Y., Prieur, D., and Appriou, P.: The rainbow vent fluids (36 degrees 14' N, MAR): the influence of ultramafic rocks and phase separation on trace metal content in Mid-Atlantic Ridge hydrothermal fluids, Chem Geol, 184, 37-48, https://doi.org/10.1016/S0009-2541(01)00351-5, 2002.

Edmond, J.M. Campell, A.C., Palmer, M.R., Klinkhammer, G.P., German, C.R., Edmonds, H.N., Elderfield, H., Thompson, G. and Rona, P.: Time series studies of vent fluids from the TAG and MARK sites (1986, 1990) Mid-Atlantic Ridge: a new solution chemistry model and a mechanisms for Cu/Zn zonation in massive sulphide orebodies, Geological Society, London, Special Publications, 87, 77-86, https://doi.org/10.1144/GSL.SP.1995.087.01.07, 1995.

Edmonds, H. N., and German, C. R.: Particle geochemistry in the Rainbow hydrothermal plume, Mid-Atlantic Ridge, Geochim Cosmochim Ac, 68, 759-772, https://doi.org/10.1016/S0016-7037(03)00498-8, 2004.

Emery, W. J., and Meincke, J.: Global Water Masses - Summary and Review, Oceanol Acta, 9, 383-391, 0399-1784/86/04, 1986.

Findlay, A. J., Gartman, A., Shaw, T. J., and Luther, G. W.: Trace metal concentration and partitioning in the first 1.5 m of hydrothermal vent plumes along the Mid-Atlantic Ridge: TAG, Snakepit, and Rainbow, Chem Geol, 412, 117-131, https://doi.org/10.1016/j.chemgeo.2015.07.021, 2015.

Fouquet, Y., Barriga, F., Charlou, J. L., Elderfield, H., German, C. R., Ondréas, H., Parson, L., Radford-Knoery, J., Relvas, J., Ribeiro, A., Schultz, A., Apprioual, R., Cambon, P., Costa, I., Donval, J. P., Douville, E., Landuré, J. Y., Normund, A., Pellé, H., Ponsevera, E., Riches, S., Santana, H., and Stephan, M.: Flores diving cruise with the Nautile near the Azores. First dives on the Rainbow field: hydrothermal seawater/mantle interaction, InterRidge News, 7, 24-28, 1998.

Frank, K. L., Rogers, D. R., Olins, H. C., Vidoudez, C., and Girguis, P. R.: Characterizing the distribution and rates of microbial sulfate reduction at Middle Valley hydrothermal vents, Isme J, 7, 1391-1401, https://doi.org/10.1038/ismej.2013.17, 2013.

734 German, C. R., Campbell, A. C., and Edmond, J. M.: Hydrothermal Scavenging at the Mid-Atlantic Ridge -
735 Modification of Trace-Element Dissolved Fluxes, Earth and Planetary Science Letters, 107, 101-114,
736 https://doi.org/10.1016/0012-821X(91)90047-L, 1991.

737 German, C. R., Klinkhammer, G. P., and Rudnicki, M. D.: The Rainbow hydrothermal plume, 36 degrees 15'N,
738 MAR, Geophys Res Lett, 23, 2979-2982, https://doi.org/10.1029/96GL02883, 1996.

739 German, C. R., Richards, K. J., Rudnicki, M. D., Lam, M. M., Charlou, J. L., and Party, F. S.: Topographic control
740 of a dispersing hydrothermal plume, Earth and Planetary Science Letters, 156, 267-273,
741 https://doi.org/10.1016/S0012-821X(98)00020-X, 1998.

742 Gwyther, D., and Wright, M.: Environmental Impact Statement: Solwara 1, Coffey Natural Systems Pty Ltd, 47-
743 65, 2008.

744 Han, Y. C., Gonnella, G., Adam, N., Schippers, A., Burkhardt, L., Kurtz, S., Schwarz-Schampera, U., Franke, H.,
745 and Perner, M.: Hydrothermal chimneys host habitat-specific microbial communities: analogues for studying the
746 possible impact of mining seafloor massive sulfide deposits, Sci Rep-Uk, 8, https://doi.org/10.1038/s41598-018-
747 28613-5, 2018.

748 Huber, J. A., Butterfield, D. A. and Baross, J. A.: Bacterial diversity in a subseafloor habitat following a deep-sea
749 volcanic eruption. FEMS Microbiol Ecol, 43(3), pp.393-409, https://doi.org/10.1111/j.1574-6941.2003.tb01080.x,
750 2003.

751 Hoagland, P., Beaulieu, S., Tivey, M. A., Eggert, R. G., German, C., Glowka, L., and Lin, J.: Deep-sea mining of
752 seafloor massive sulfides, Mar Policy, 34, 728-732, https://doi.org/10.1016/j.marpol.2009.12.001, 2010.

753 Jannasch, H. W., and Mottl, M. J.: Geomicrobiology of Deep-Sea Hydrothermal Vents, Science, 229, 717-725,
754 https:/doi.org/10.1126/science.229.4715.717, 1985.

755 Jones, D. O. B., Amon, D. L., and Chapman, A. S. A.: Mining Deep-Ocean Mineral Deposits: What are the
756 Ecological Risks?, Elements, 14, 325-330, https://doi.org/10.2138/gselements.14.5.325, 2018.

757 Khripounoff, A., Vangriesheim, A., Crassous, P., Segonzac, M., Colaco, A., Desbruyeres, D., and Barthelemy, R.:
758 Particle flux in the Rainbow hydrothermal vent field (Mid-Atlantic Ridge): Dynamics, mineral and biological
759 composition, J Mar Res, 59, 633-656, https://doi.org/10.1357/002224001762842217, 2001.

760 Levin, L. A., Mengerink, K., Gjerde, K. M., Rowden, A. A., Van Dover, C. L., Clark, M. R., Ramirez-Llodra, E.,
761 Currie, B., Smith, C. R., Sato, K. N., Gallo, N., Sweetman, A. K., Lily, H., Armstrong, C. W., and Brider, J.:
762 Defining "Serious Harm" to the Marine Environment in the Context of Deep-Seabed Mining, Marine Policy, 245-
763 59, http://dx.doi.org/10.1016/j.marpol.2016.09.032, 2016

764 López-García, P., Duperron, S., Philippot, P., Foriel, J., Susini, J., & Moreira, D.: Bacterial diversity in
765 hydrothermal sediment and epsilonproteobacterial dominance in experimental microcolonizers at the Mid-Atlantic
766 Ridge. Environmental Microbiology, 5(10), 961-976, https://doi.org/10.1046/j.1462-2920.2003.00495.x, 2003.

767 Ludford, E. M., Palmer, M. R., German, C. R., and Klinkhammer, G. P.: The geochemistry of Atlantic hydrothermal
768 particles, Geophys Res Lett, 23, 3503-3506, https://doi.org/10.1029/96GL02078, 1996.

769 Mandernack, K. W., and Tebo, B. M.: Manganese Scavenging and Oxidation at Hydrothermal Vents and in Vent
770 Plumes, Geochim Cosmochim Ac, 57, 3907-3923, https://doi.org/10.1016/0016-7037(93)90343-U, 1993.

771 Marques, A. F. A., Barriga, F., Chavagnac, V. and Fouquet, Y. : Mineralogy, geochemistry, and Nd isotope
772 composition of the Rainbow hydrothermal field, Mid-Atlantic Ridge, Mineralium Deposita, 41, 52-67,
773 https://doi.org/10.007/s00126-005-0040-8, 2006.

774 McCollom, T. M.: Geochemical constraints on primary productivity in submarine hydrothermal vent plumes, Deep-
775 Sea Res Pt I, 47, 85-101, https://doi.org/10.1016/S0967-0637(99)00048-5, 2000.

776 Michard, G., Albarède, F., Michard, A., Minister, J. F., Charlou. J. L., and Tan, N.: Chemistry of Solution from the
777 13 degrees N East Pacific Rise Hydrothermal Site. Earth and Planetary Science Letters 67, 297-307,
778 https://doi.org/10.1016/0012-821X(84)90169-9, 1984

779 Mino, S., Nakagawa, S., Makita, H., Toki, T., Miyazaki, J., Sievert, S. M., ... & Watanabe, H.: Endemicity of the
780 cosmopolitan mesophilic chemolithoautotroph Sulfurimonas at deep-sea hydrothermal vents. The ISME journal,
781 11(4), 909, https://doi.org/10.1038/ismej.2016.178, 2017.

782 Nakagawa, S., Takai, K., Inagaki, F., Hirayama, H., Nunoura, T., Horikoshi, K., and Sako, Y.: Distribution,
783 phylogenetic diversity and physiological characteristics of epsilon-Proteobacteria in a deep-sea hydrothermal field,
784 Environ Microbiol, 7, 1619-1632, https://doi.org/10.1111/j.1462-2920.2005.00856.x, 2005.

785 Olins, H. C., Rogers, D. R., Preston, C., Ussler, W., Pargett, D., Jensen, S., Roman, B., Birch, J. M., Scholin, C.
786 A., Haroon, M. F., and Girguis, P. R.: Co-registered Geochemistry and Metatranscriptomics Reveal Unexpected

787 Distributions of Microbial Activity within a Hydrothermal Vent Field, Front Microbiol, 8,
788 https://doi.org/10.3389/fmicb.2017.01042, 2017.

789 Opatkiewicz, A. D., Butterfield, D. A., and Baross, J. A.: Individual hydrothermal vents at Axial Seamount harbor
790 distinct subseafloor microbial communities, Fems Microbiol Ecol, 70, 413-424, https://doi.org/10.1111/j.1574-
791 6941.2009.00747.x, 2009.

792 Orcutt, B. N., Sylvan, J. B., Knab, N. J., & Edwards, K. J.: Microbial ecology of the dark ocean above, at, and
793 below the seafloor. Microbiol. Mol. Biol. Rev., 75(2), 361-422, https://doi.org/10.1128/MMBR.00039-10, 2011.

794 Phillips, B. T.: Beyond the vent: New perspectives on hydrothermal plumes and pelagic biology, Deep-Sea Res Pt
795 Ii, 137, 480-485, https://doi.org/10.1016/j.dsr2.2016.10.005, 2017.

796 Ramirez-Llodra, E., Tyler, P. A., Baker, M. C., Bergstad, O. A., Clark, M. R., Escobar, E., Levin, L. A., Menot,
797 L., Rowden, A. A., Smith, C. R., and Van Dover, C. L.: Man and the Last Great Wilderness: Human Impact on the
798 Deep Sea, Plos One, 6, https://doi.org/10.1371/journal.pone.0022588, 2011.

799 Reed, D. C., Breier, J. A., Jiang, H. S., Anantharaman, K., Klausmeier, C. A., Toner, B. M., Hancock, C., Speer,
800 K., Thurnherr, A. M., and Dick, G. J.: Predicting the response of the deep-ocean microbiome to geochemical
801 perturbations by hydrothermal vents, Isme J, 9, 1857-1869, https://doi.org/10.1038/ismej.2015.4, 2015.

802 Resing, J. A., P. N. Sedwick, C. R. German, W. J. Jenkins, J. W. Moffett, B. M. Sohst, and A. Tagliabue.: Basin-
803 Scale Transport of Hydrothermal Dissolved Metals across the South Pacific Ocean. Nature 523, no. 7559, 200-3.
804 http://dx.doi.org/10.1038/nature14577, 2015.

805 Severmann, S., Johnson, C. M., Beard, B. L., German, C. R., Edmonds, H. N., Chiba, H., and Green, D. R. H.: The
806 effect of plume processes on the Fe isotope composition of hydrothermally derived Fe in the deep ocean as inferred
807 from the Rainbow vent site, Mid-Atlantic Ridge, 36 degrees 14' N, Earth and Planetary Science Letters, 225, 63-
808 76, https://doi.org/10.1016/j.epsl.2004.06.001, 2004.

809 Sheik, C. S., Anantharaman, K., Breier, J. A., Sylvan, J. B., Edwards, K. J., and Dick, G. J.: Spatially resolved
810 sampling reveals dynamic microbial communities in rising hydrothermal plumes across a back-arc basin, Isme J,
811 9, 1434-1445, https://doi.org/10.1038/ismej.2014.228, 2015.

812 Sunamura, M., Higashi, Y., Miyako, C., Ishibashi, J., and Maruyama, A.: Two bactetia phylotypes are predominant
813 in the Suiyo Seamount hydrothermal plume, Appl Environ Microb, 70, 1190-1198,
814 https://doi.org/10.1128/AEM.70.2.1190-1198.2004, 2004.

815 Sylvan, J. B., Pyenson, B. C., Rouxel, O., German, C. R., & Edwards, K. J.: Time-series analysis of two
816 hydrothermal plumes at 9° 50′ N East Pacific Rise reveals distinct, heterogeneous bacterial populations.
817 Geobiology, 10(2), 178-192, https://doi.org/10.1111/j.1472-4669.2011.00315.x, 2012.

818 Thurnherr, A. M., and Richards, K. J.: Hydrography and high-temperature heat flux of the Rainbow hydrothermal
819 site (36 degrees 14 ' N, Mid-Atlantic Ridge), J Geophys Res-Oceans, 106, 9411-9426,
820 https://doi.org/10.1029/2000JC900164, 2001.

821 Thurnherr, A. M., Richards, K. J., German, C. R., Lane-Serff, G. F., and Speer, K. G.: Flow and mixing in the rift
822 valley of the Mid-Atlantic Ridge, J Phys Oceanogr, 32, 1763-1778, https://doi.org/10.1175/1520-
823 0485(2002)032<1763:FAMITR>2.0.CO;2, 2002.

824 Trocine, R. P. and Trefry, J. H.: Distribution and chemistry of suspended particles from an active hydrothermal
825 vent site on the Mid-Atlantic Ridge at 26 °N, Earth and Planetary Science Letters 88, 1-15,
826 https://doi.org/10.1016/0012-821X(88)90041-6, 1988.

827 van Bleijswijk, J. D. L., Whalen, C., Duineveld, G. C. A., Lavaleye, M. S. S., Witte, H. J., and Mienis, F.: Microbial
828 assemblages on a cold-water coral mound at the SE Rockall Bank (NE Atlantic): interactions with hydrography
829 and topography, Biogeosciences, 12, 4483-4496, https://doi.org/10.5194/bg-12-4483-2015, 2015.

830 van Haren, H., Duineveld, G., and de Stigter, H.: Prefrontal bore mixing, Geophys Res Lett, 44, 9408-9415,
831 https://doi.org/10.1002/2017GL074384, 2017.

832 Vare, L. L., Baker, M. C., Howe, J. A., Levin, L. A., Neira, C., Ramirez-Llodra, E. Z., Reichelt-Brushett, A.,
833 Rowden, A. A., Shimmield, T. M., Simpson, S. L., and Soto, E. H.: Scientific Considerations for the Assessment
834 and Management of Mine Tailings Disposal in the Deep Sea, Frontiers in Marine Science, 5,
835 https://doi.org/10.3389/fmars.2018.00017, 2018.

836 Weaver, P. P., Billett, D. S., and Van Dover, C. L.: Environmental risks of deep-sea mining, in: Handbook on
837 Marine Environment Protection, Springer, 215-245, https://doi.org/10.1007/978-3-319-60156-4_11, 2018.

838 Wetzel, L. R., and Shock, E. L.: Distinguishing ultramafic- from basalt-hosted submarine hydrothermal systems
839 by comparing calculated vent fluid compositions, J Geophys Res-Sol Ea, 105, 8319-8340,
840 https://doi.org/10.1029/1999JB900382, 2000.

841 Yilmaz, P., Parfrey, L.W., Yarza, P., Gerken, J., Pruesse, E., Quast, C., Schweer, T., Peplies, J., Ludwig, W. and
842 Glöckner, F.O.: The SILVA and "all-species living tree project (LTP)" taxonomic frameworks. Nucleic Acids Res,
843 42(D1), pp.D643-D648, https://doi.org/10.1093/nar/gkt1209, 2014.

844 Zinger, L., Amaral-Zettler, L. A., Fuhrman, J. A., Horner-Devine, M. C., Huse, S. M., Welch, D. B. M., Martiny,
845 J. B. H., Sogin, M., Boetius, A., and Ramette, A.: Global Patterns of Bacterial Beta-Diversity in Seafloor and
846 Seawater Ecosystems, Plos One, 6, https://doi.org/10.1371/journal.pone.0024570, 2011.

847

848

849

Figures and tables

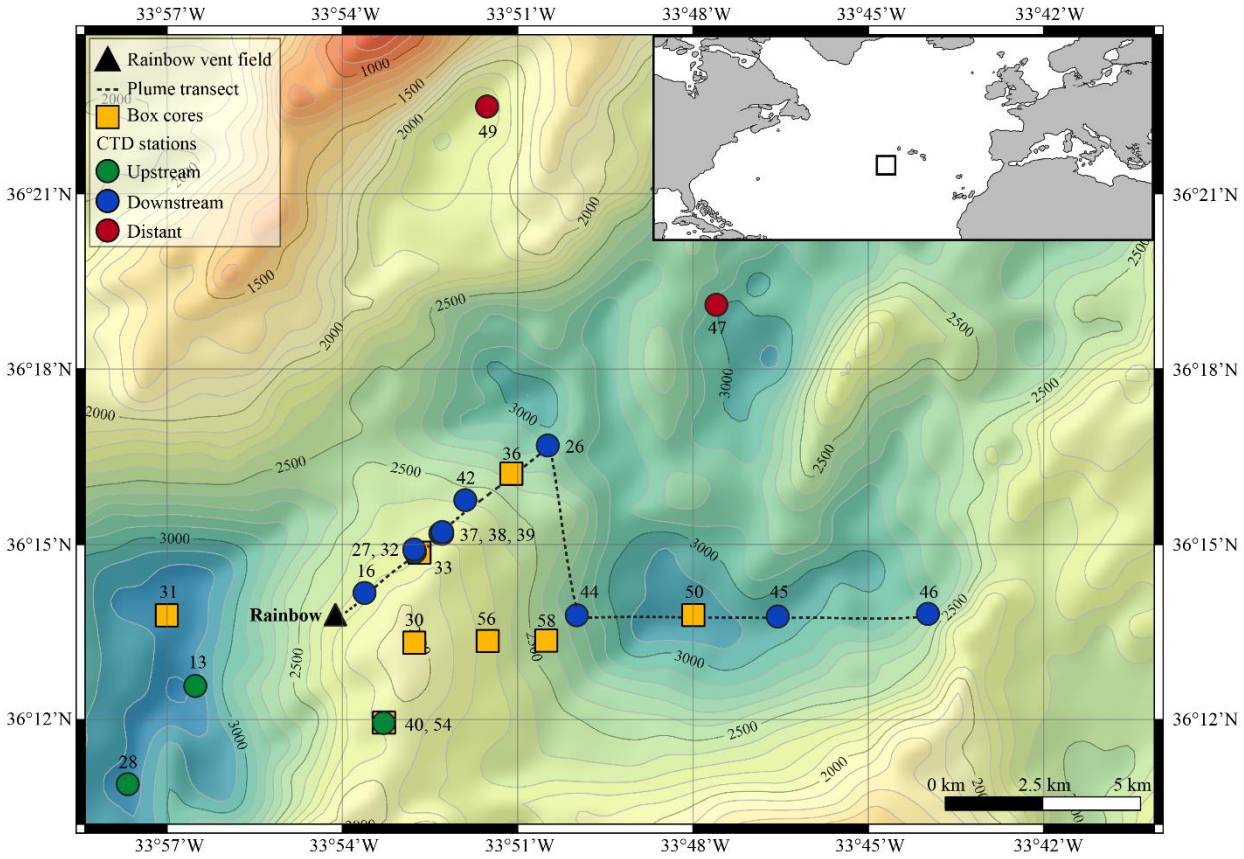

Figure 1: Geographical location (inset) and bathymetric map of the Rainbow study site on the Mid Atlantic Ridge (from EMOD data base) with sampling locations depicted.

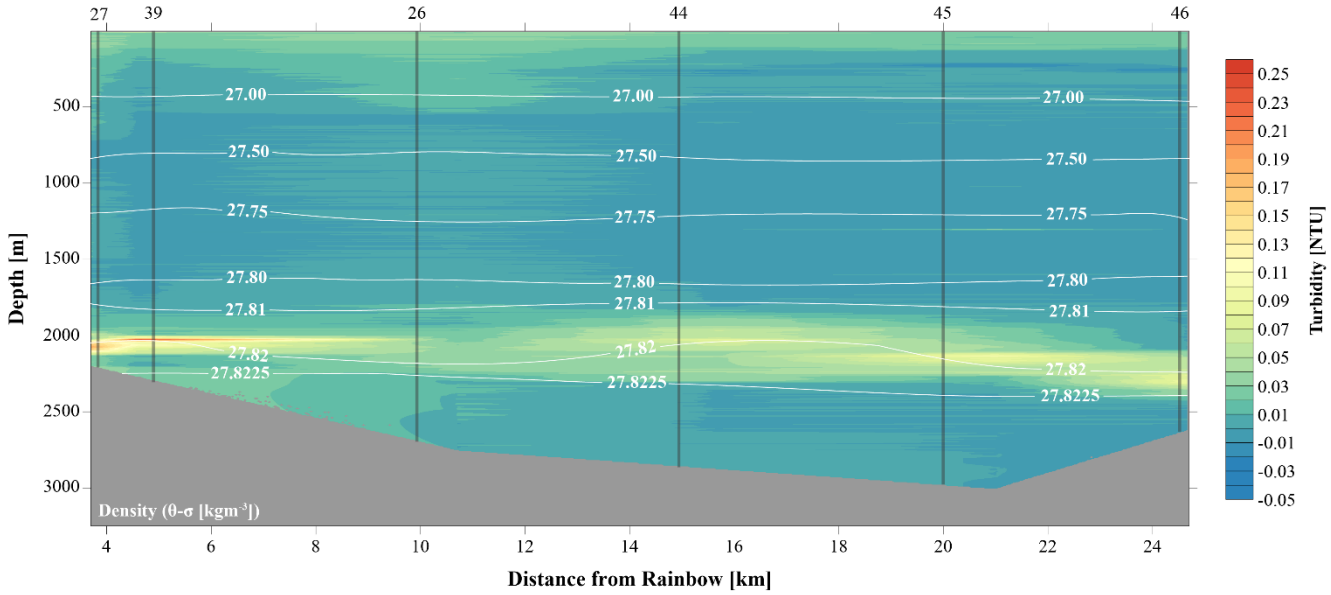

Figure 2: Transect along main plume path (indicated in Fig. 1 as plume transect), showing turbidity in the water column. The plume is indicated by highest turbidity values and disperses away from the Rainbow vent field.

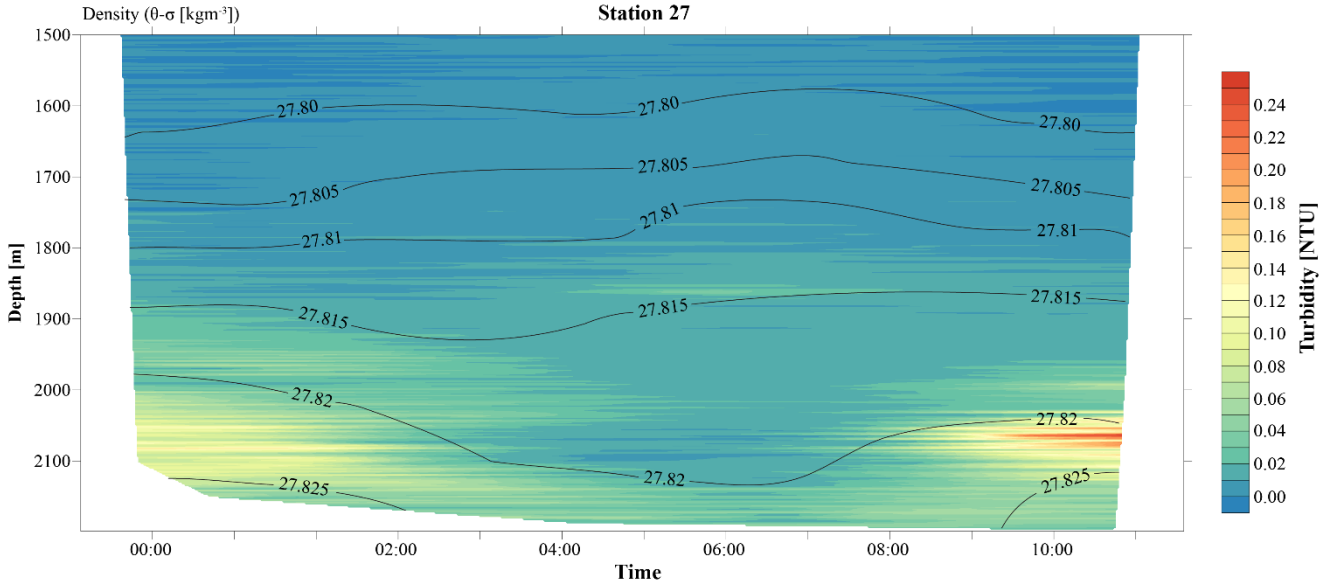

Figure 3: A 12 hour yoyo CTD at station 27 showing the temporal evolution of the hydrothermal plume over a tidal cycle.

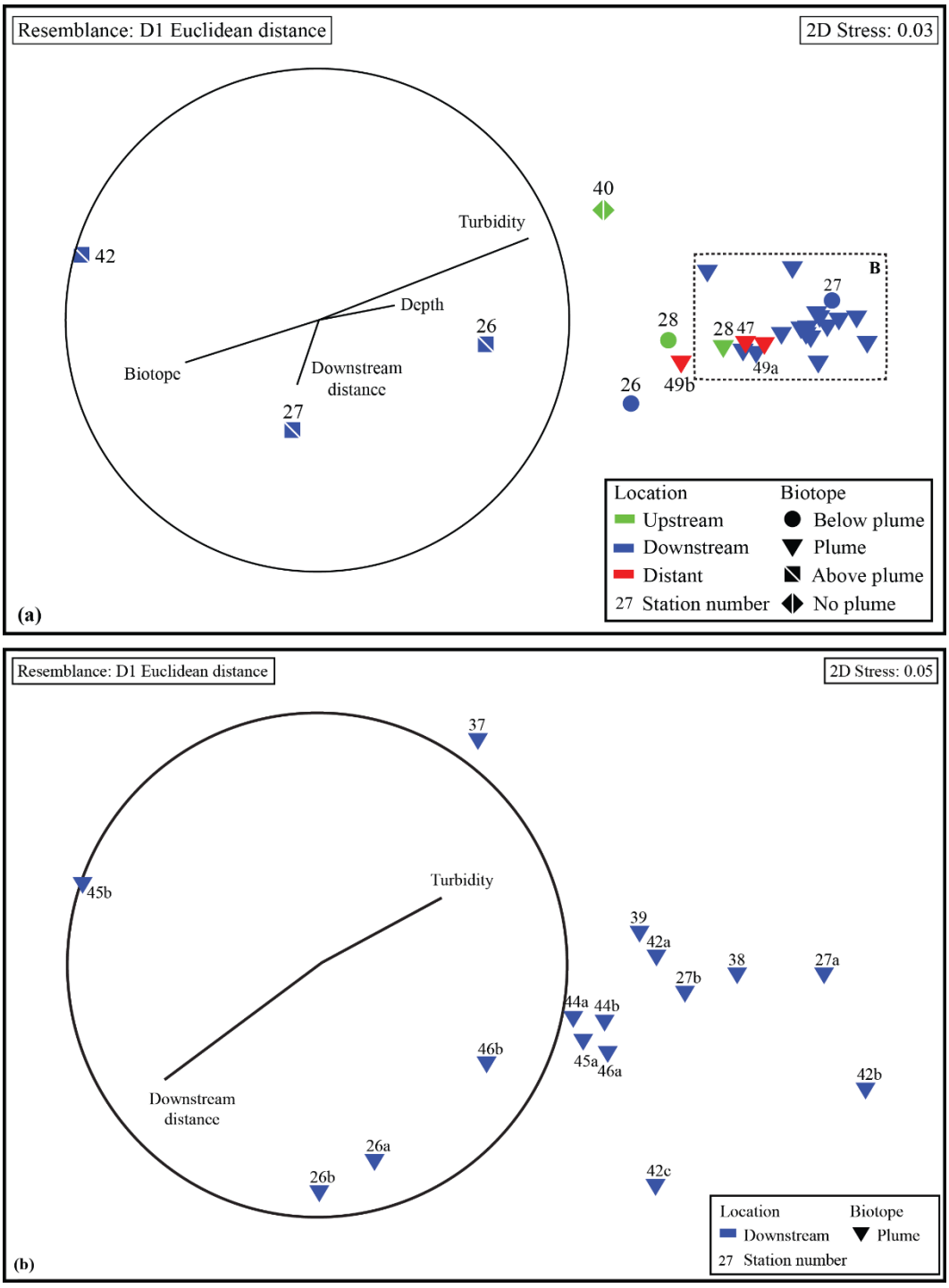

Figure 4: (a) NMDS ordination showing all water samples based on their resemblance in chemical composition. (b) NMDS ordination showing all plume samples from the downstream stations based on their resemblance in chemical composition.

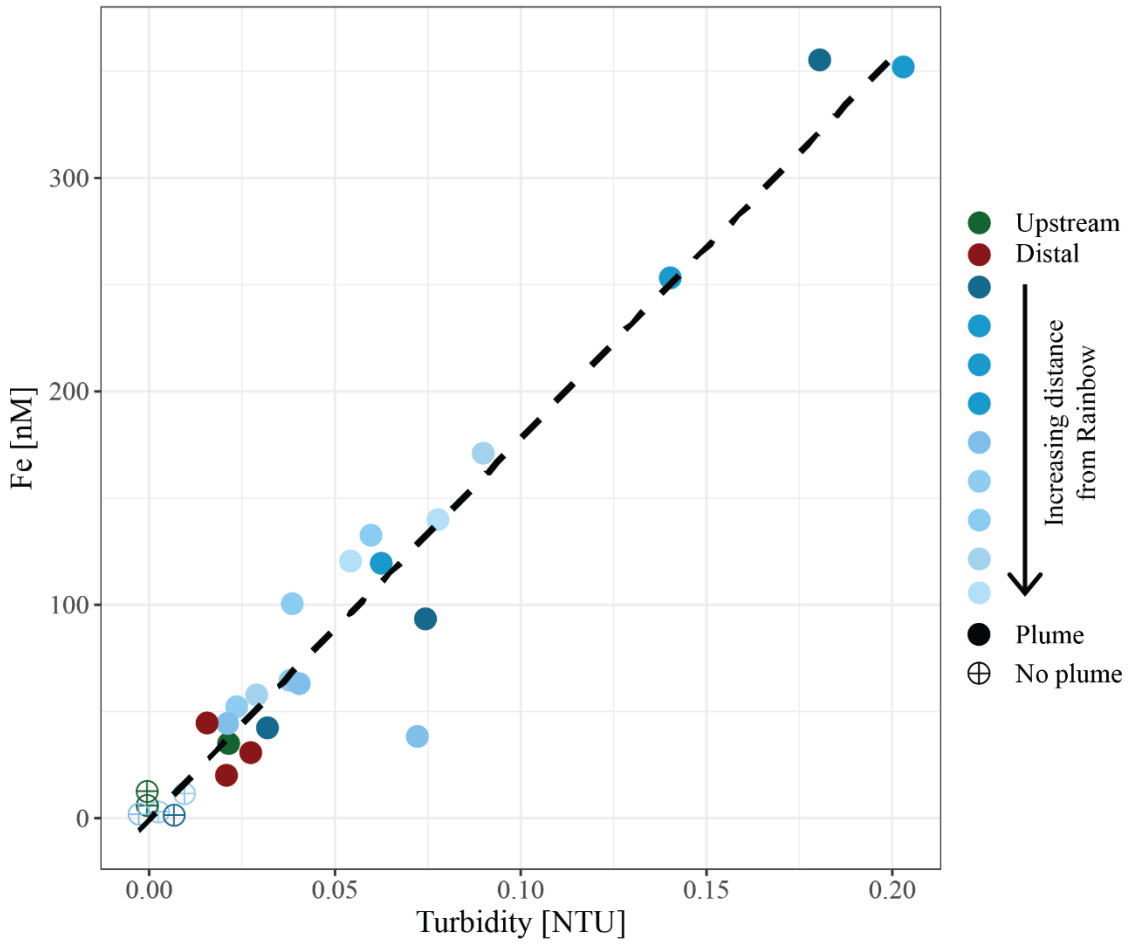

Figure 5: Relationship between in-situ measured turbidity and molar concentration of particulate iron.

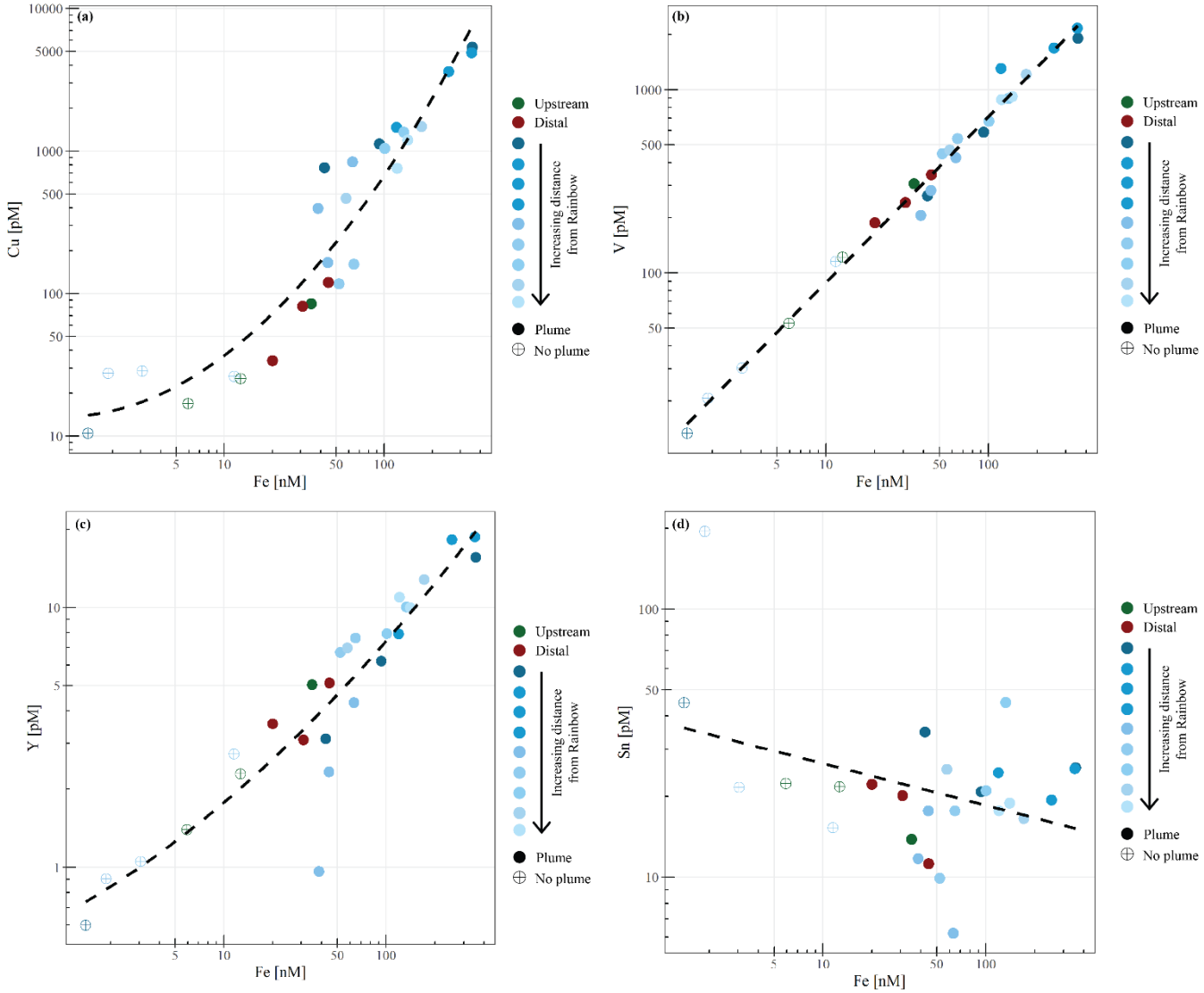

870

871 *Figure 6: Relationships between molar concentrations of particulate copper (a), vanadium (b), yttrium (c) and*
872 *tin (d) to iron.*

873

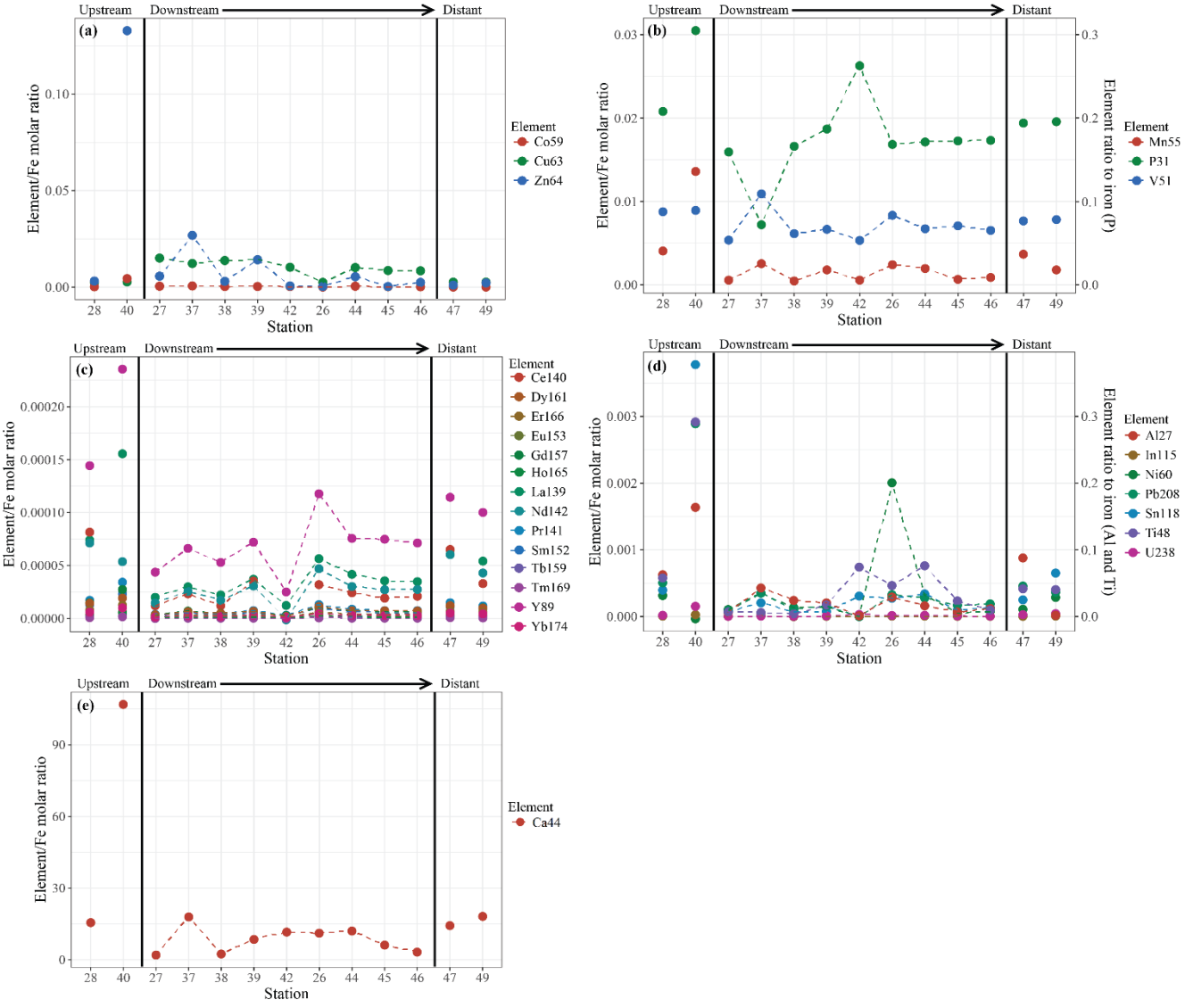

Figure 7: Element to iron molar ratios of plume samples of upstream, downstream and distant stations. Downstream stations follow the main path of the plume. (a) shows the element/Fe molar ratios of the chalcophiles (Co, Cu and Zn), (b) shows the ratios of Mn and the oxyanions (P and V), (c) displays the ratios of REEs, (d) the ratios of Al, In, Ni, Pb, Sn, Ti and U and (e) shows the Ca/Fe molar ratios.

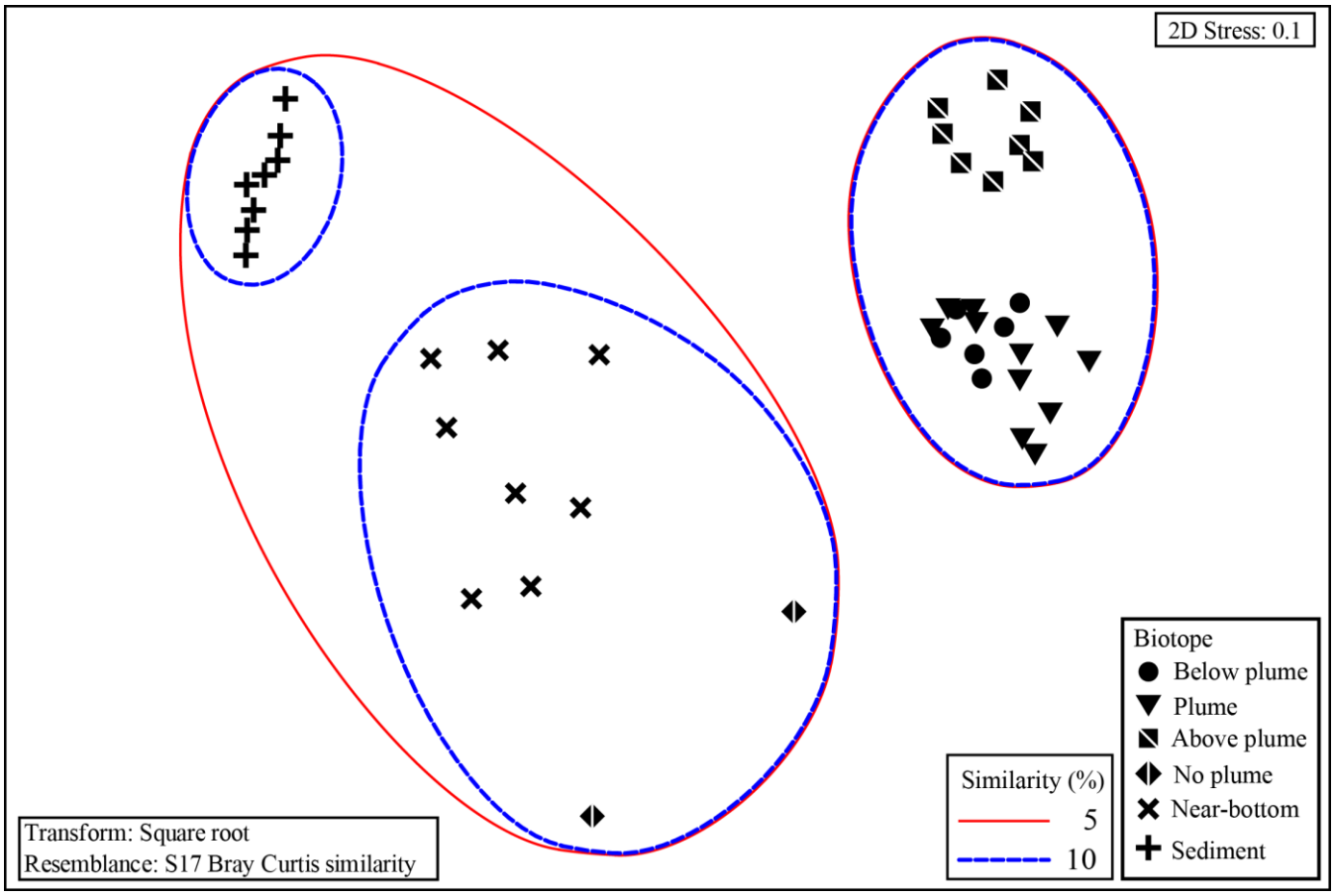

Figure 8: Non-metric multidimensional scaling plot of the microbial community composition of all samples based on Operational Taxonomic units. Similarity groupings are based on group average clustering. "No plume" is representative of samples collected from station 13, where there was no indication of a plume.

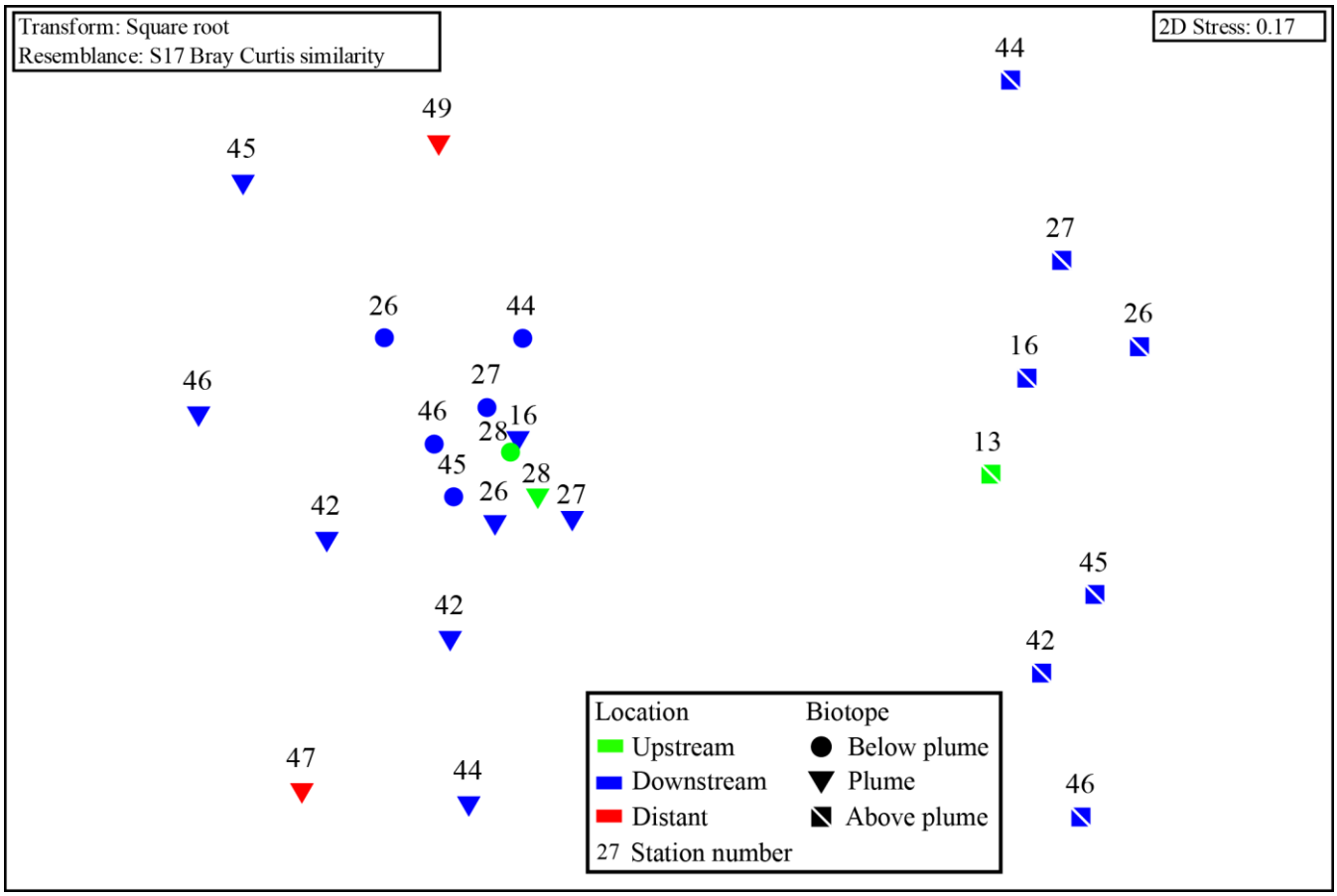

Figure 9: Non-metric multidimensional scaling plot of the microbial community composition of all water column samples based on Operational Taxonomic units. Plume and below plume depths from Station 13 were excluded.

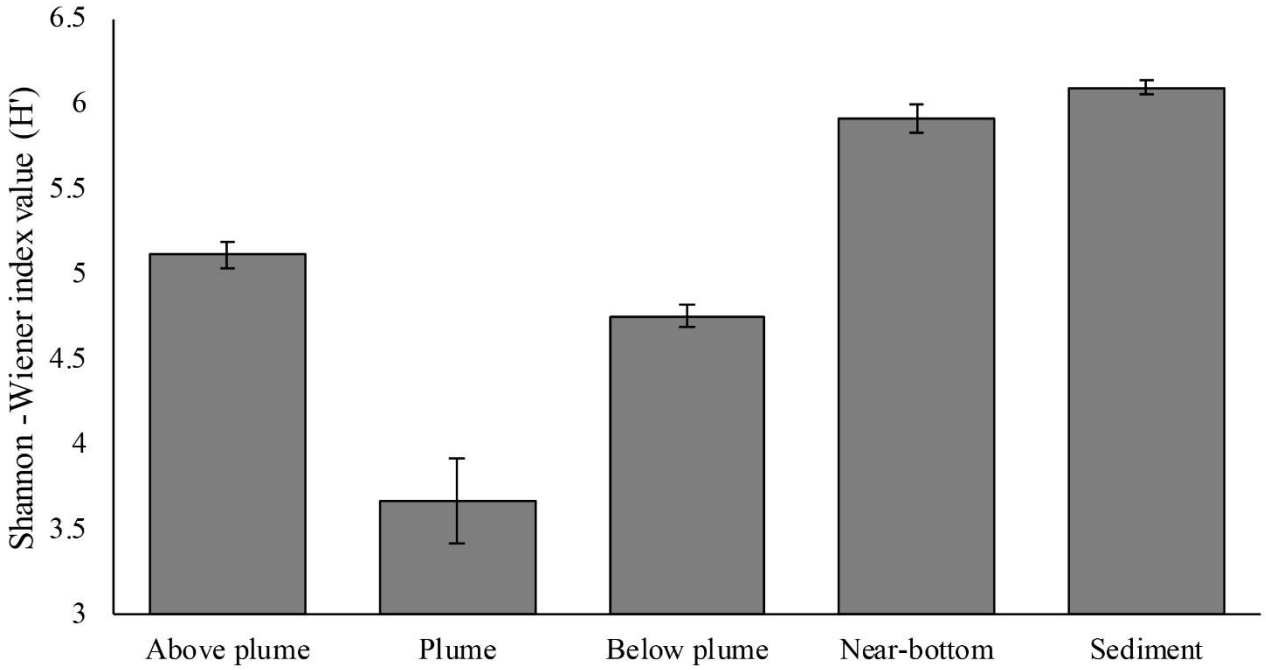

Figure 10: Mean Shannon-Wiener diversity index for microorganisms in each biotope. Error bars represent ±SE

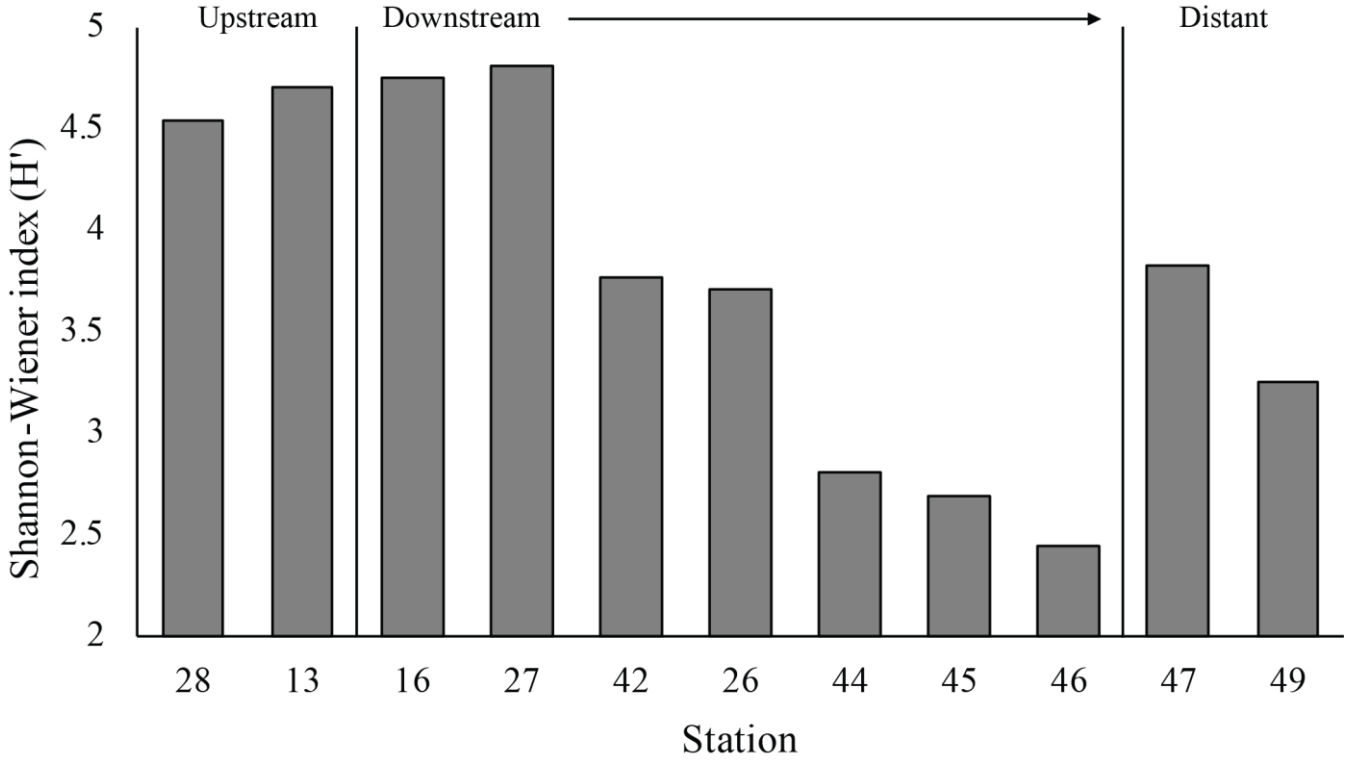

892

893 *Figure 11: Shannon-Wiener index values for microorganisms in each plume sample taken.*

894

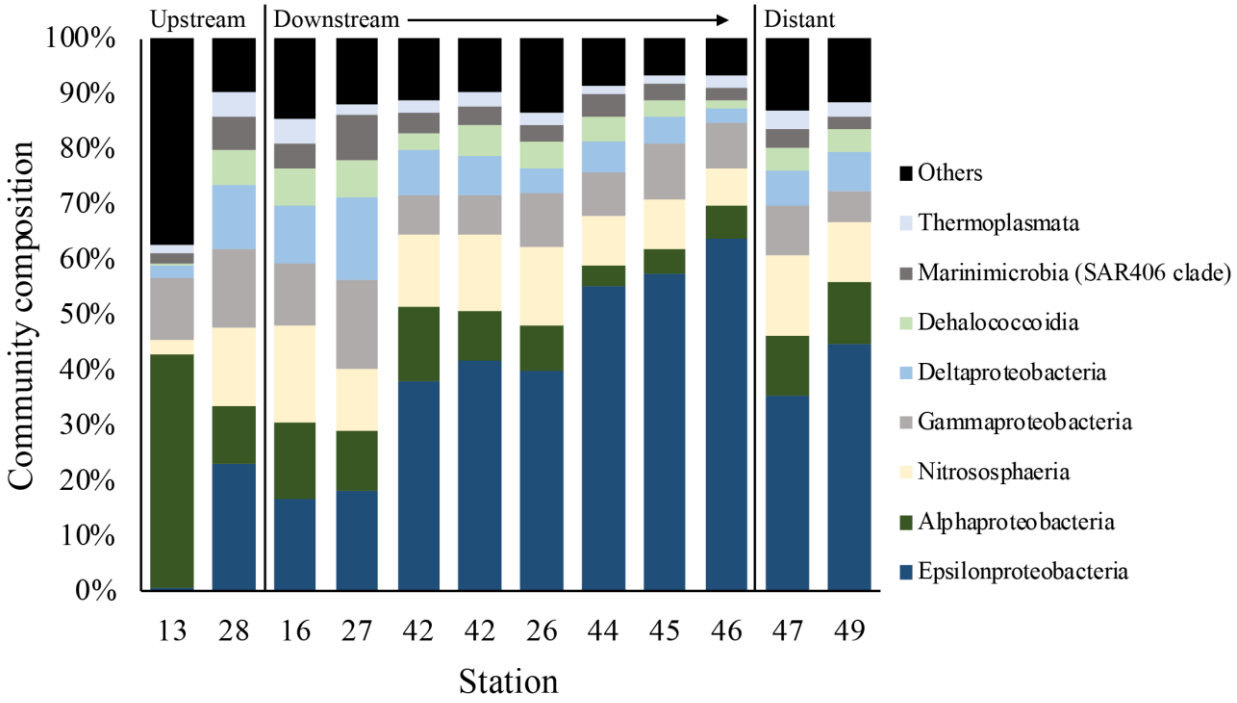

Figure 12: Microbial community composition in the plume samples as a percentage of the dominant class groups in accordance with the SIMPER results.

899 *Table 1: Meta-data of samples taken.*

Station	Latitude	Longitude	Biotope	Sample type	Depth (m)	Micro-biology	SPM	(Trace) metals
30	36°13’19”N	33°52’46”W	Sediment and near-bottom water	Box core	1970	x		
31	36°13’47”N	33°57’00”W	Sediment and near-bottom water	Box core	3190	x		
33	36°14’51”N	33°52’41”W	Sediment and near-bottom water	Box core	2223	x		
36	36°16’13”N	33°51’06”W	Sediment and near-bottom water	Box core	2857	x		
50	36°13’47”N	33°47’60”W	Sediment and near-bottom water	Box core	3157	x		
54	36°11’57”N	33°53’46”W	Sediment and near-bottom water	Box core	2129	x		
56	36°13’21”N	33°51’31”W	Sediment and near-bottom water	Box core	2198	x		
58	36°13’21”N	33°50’31”W	Sediment and near-bottom water	Box core	2514	x		
13	36°12’35”N	33°56’31”W	Above plume	CTD	125	x		
13	36°12’35”N	33°56’31”W	Below plume	CTD	3220	x		
13	36°12’35”N	33°56’31”W	Plume	CTD	2000	x		
16	36°14’10”N	33°53’37”W	Plume	CTD	1944	x		
16	36°14’10”N	33°53’37”W	Above plume	CTD	998	x		
26	36°16’41”N	33°50’29”W	Below plume	CTD	2756	x	x	x
26	36°16’41”N	33°50’29”W	Plume	CTD	2150	x	x	x
26	36°16’41”N	33°50’29”W	Plume	CTD	2000		x	x
26	36°16’41”N	33°50’29”W	Above plume	CTD	999	x	x	x
27	36°16’52”N	33°52’45”W	Below plume	CTD	2191	x		x
27	36°16’52”N	33°52’45”W	Plume	CTD	2077	x		x
27	36°16’52”N	33°52’45”W	Plume	CTD	1996			x
27	36°16’52”N	33°52’45”W	Above plume	CTD	994	x		x
28	36°10’54”N	33°57’40”W	Below plume	CTD	3170	x	x	x
28	36°10’54”N	33°57’40”W	Plume	CTD	1975	x	x	x
32	36°14’55”N	33°52’46”W	Plume	CTD	2192		x	
32	36°14’55”N	33°52’46”W	Plume	CTD	2088		x	
37	36°15’11”N	33°52’19”W	Plume	CTD	2190			x
38	36°15’11”N	33°52’17”W	Plume	CTD	2040			x
39	36°15’13”N	33°52’17”W	Plume	CTD	2019			x
40	36°11’57”N	33°53’18”W	No plume	CTD	2120			x
42	36°15’45”N	33°51’54”W	Plume	CTD	2291	x	x	x
42	36°15’45”N	33°51’54”W	Plume	CTD	2209	x	x	x
42	36°15’45”N	33°51’54”W	Plume	CTD	2037		x	x
42	36°15’45”N	33°51’54”W	Above plume	CTD	999	x	x	x
44	36°13’47”N	33°49’59”W	Below plume	CTD	2623	x		
44	36°13’47”N	33°49’59”W	Plume	CTD	2202		x	x
44	36°13’47”N	33°49’59”W	Plume	CTD	2002	x	x	x
44	36°13’47”N	33°49’59”W	Above plume	CTD	995	x		
45	36°13’46”N	33°46’33”W	Below plume	CTD	3004	x		
45	36°13’46”N	33°46’33”W	Plume	CTD	2166		x	x
45	36°13’46”N	33°46’33”W	Plume	CTD	2002	x	x	x
45	36°13’46”N	33°46’33”W	Above plume	CTD	996	x		
46	36°13’49”N	33°43’59”W	Below plume	CTD	2622	x		
46	36°13’49”N	33°43’59”W	Plume	CTD	2280	x	x	x
46	36°13’49”N	33°43’59”W	Plume	CTD	2145		x	x
46	36°13’49”N	33°43’59”W	Above plume	CTD	1000	x		
47	36°19’06”N	33°47’36”W	Below plume	CTD	2850			
47	36°19’06”N	33°47’36”W	Plume	CTD	2200	x		x
49	36°22’19”N	33°51’31”W	Plume	CTD	2260	x	x	x
49	36°22’19”N	33°51’31”W	Plume	CTD	1902		x	x

900

901 *Table 2: Primers used for sequencing.*

Forward		Reverse			
Primer name	Primer sequence 5'-3'	Primer name	Primer sequence 5'-3'	Ratio in mix	Reference
Arch-0519-a-S-1 (universal)	CAGCMGCCGCGGTAA	Bact-0785-b-A-18 (universal)	TACNVGGGTATCTAATCC	3/9 + 3/9	Klindworth et al. 2012
Bact-0519F (targets WS6, TM7, OP11	CAGCAGCATCGGTVA			1/9	This paper
Nano-0519F (targets Nanoarchaea)	CAGTCGCCRCGGGAA	Nano-0785R (targets Nanoarchaea)	TACNVGGGTMTCTAATYY	1/9+1/9	This paper

902

903

904 *Table 3: SIMPER similarity results of each biotope at class level. ** indicates undefined class.*

Biotope	Average similarity (%)	Class	Average proportion (%)	Average similarity	Sim/SD	Contribution (%)	Cumulative %
Above plume	82.34	Nitrososphaeria	27.10	22.79	4.61	27.67	27.67
		Alphaproteobacteria	18.34	15.22	4.15	18.49	46.16
		Gammaproteobacteria	13.44	11.58	5.52	14.07	60.23
		Deltaproteobacteria	10.67	8.46	3.38	10.27	70.50
		Marinimicrobia (SAR406 clade)	8.22	6.96	6.07	8.46	78.96
		Dehalococcoidia	6.38	5.69	9.19	6.91	85.87
		Thermoplasmata	2.63	2.26	5.68	2.74	88.61
		Acidimicrobiia	2.13	1.89	8.62	2.30	90.91
Plume	76.74	Epsilonproteobacteria	39.59	30.29	2.53	39.47	39.47
		Nitrososphaeria	12.16	10.32	4.05	13.45	52.92
		Gammaproteobacteria	9.69	7.92	4.71	10.32	63.23
		Alphaproteobacteria	9.23	7.22	2.44	9.40	72.64
		Deltaproteobacteria	7.60	5.56	2.75	7.25	79.88
		Dehalococcoidia	4.57	3.55	2.58	4.63	84.51
		Marinimicrobia (SAR406 clade)	4.02	3.07	3.83	4.00	88.51
		Thermoplasmata	2.56	1.94	3.39	2.53	91.04
Below plume	77.94	Nitrososphaeria	22.35	16.60	3.29	21.30	21.30
		Alphaproteobacteria	13.26	11.43	5.18	14.67	35.97
		Deltaproteobacteria	10.88	9.25	8.31	11.87	47.84
		Gammaproteobacteria	10.60	8.89	7.78	11.40	59.24
		Epsilonproteobacteria	9.65	7.18	2.50	9.22	68.46
		Dehalococcoidia	7.84	6.97	7.89	8.95	77.40
		Marinimicrobia (SAR406	6.32	4.49	2.31	5.76	83.16
		Thermoplasmata	4.69	3.04	2.20	3.90	87.07
		Phycisphaerae	1.97	1.75	7.60	2.24	89.31
		Planctomycetacia	2.03	1.50	2.96	1.93	91.23
Near-bottom water	75.71	Gammaproteobacteria	20.79	16.77	3.18	22.15	22.15
		Nitrososphaeria	16.90	13.54	3.79	17.89	40.04
		Alphaproteobacteria	15.55	13.25	5.47	17.50	57.54
		Deltaproteobacteria	6.68	5.89	5.99	7.78	65.32
		Oxyphotobacteria	5.93	4.04	2.18	5.34	70.66
		Dehalococcoidia	4.08	2.99	2.50	3.95	74.61
		Phycisphaerae	3.72	2.57	2.03	3.40	78.01
		Thermoplasmata	2.47	1.70	2.25	2.24	80.25
		Acidimicrobiia	2.06	1.61	2.72	2.13	82.38
		Bacteroidia	2.15	1.57	1.85	2.07	84.45
		Marinimicrobia (SAR406 clade)	1.75	1.24	2.17	1.64	86.09
		OM190	1.64	1.14	2.02	1.51	87.60
		Planctomycetacia	1.40	1.09	2.76	1.44	89.04
		Epsilonproteobacteria	1.71	0.85	1.08	1.12	90.16
Sediment	82.51	Gammaproteobacteria	29.67	27.17	8.51	32.93	32.93
		Alphaproteobacteria	13.98	12.44	4.88	15.07	48.01
		Deltaproteobacteria	11.98	10.98	10.24	13.30	61.31
		Nitrososphaeria	7.73	5.69	3.74	6.90	68.21
		Phycisphaerae	5.46	5.01	7.85	6.07	74.28
		Dehalococcoidia	3.35	2.48	2.58	3.01	77.29
		BD2-11 terrestrial group	2.36	1.91	2.90	2.31	79.60
		Subgroup 22 (Acidobacteria)	2.10	1.74	3.22	2.11	81.71
		OM190	2.09	1.50	5.50	1.81	83.53
		Nitrospira	1.79	1.49	3.68	1.80	85.33
		Bacteroidia	1.91	1.48	3.66	1.79	87.12
		Acidimicrobiia	1.58	1.24	2.84	1.50	88.62
		Thermoanaerobaculia	1.41	1.07	3.25	1.30	89.92
		Gemmatimonadetes**	1.57	1.06	1.56	1.28	91.21

905